ARTICLES
https://doi.org/10.1038/s41591-020-0971-8

nature medicine

Check for updates

Xenogeneic cross-circulation for extracorporeal recovery of injured human lungs

Ahmed E. Hozain[1,2,19], John D. O'Neill[1,19], Meghan R. Pinezich[1], Yuliya Tipograf[2], Rachel Donocoff[3], Katherine M. Cunningham[1], Andrew Tumen[4], Kenmond Fung[5], Rei Ukita[4], Michael T. Simpson[2], Jonathan A. Reimer[1,2], Edward C. Ruiz[1], Dawn Queen[6], John W. Stokes[4], Nancy L. Cardwell[4], Jennifer Talackine[4], Jinho Kim[1,7], Hans-Willem Snoeck[8,9,10], Ya-Wen Chen[8,11,12], Alexander Romanov[3], Charles C. Marboe[13], Adam D. Griesemer[2,14], Brandon A. Guenthart[1,15], Matthew Bacchetta[1,4,16,17,18,19] ✉ and Gordana Vunjak-Novakovic[1,8,19] ✉

Patients awaiting lung transplantation face high wait-list mortality, as injury precludes the use of most donor lungs. Although ex vivo lung perfusion (EVLP) is able to recover marginal quality donor lungs, extension of normothermic support beyond 6 h has been challenging. Here we demonstrate that acutely injured human lungs declined for transplantation, including a lung that failed to recover on EVLP, can be recovered by cross-circulation of whole blood between explanted human lungs and a Yorkshire swine. This xenogeneic platform provided explanted human lungs a supportive, physiologic milieu and systemic regulation that resulted in functional and histological recovery after 24 h of normothermic support. Our findings suggest that cross-circulation can serve as a complementary approach to clinical EVLP to recover injured donor lungs that could not otherwise be utilized for transplantation, as well as a translational research platform for immunomodulation and advanced organ bioengineering.

Medical, surgical and technological advancements in organ transplantation continue to expand life-saving treatment options for patients with end-stage lung disease, but transplantation remains limited by the low availability of donor organs. As chronic respiratory disease is the third-leading cause of death worldwide[1], the need for innovative solutions to reduce associated morbidity and mortality is imperative. In 2020, lung transplantation remains the only definitive cure for end-stage lung disease, which has poor prognosis due to disease severity, insufficient donor lung availability[2] and high rates of chronic allograft dysfunction[3,5].

Strategies to increase organ supply involve utilizing extended criteria lungs[4], developing new technologies to recover donor lungs for transplantation[5,6] and generating transplantable organs from xenogeneic sources, such as genetically engineered swine[7,8]. Currently, the most utilized approach is to recover standard and extended criteria lungs by normothermic EVLP[9]. However, evidence of cellular regeneration in injured human lungs has not been robustly demonstrated in EVLP studies. To increase the quality and duration of extracorporeal lung support and investigate the potential for cellular regeneration, our group previously reported the development of an organ support platform in a swine model[10]. While EVLP of healthy swine lungs perfused with whole blood has been reported[11,12], a study of injured swine lungs placed on EVLP with whole blood demonstrated insufficient recovery and resulted in impaired oxygenation and poor performance after transplantation[13]. In contrast, cross-circulation of severely injured swine lungs with a swine host enabled substantial cellular regeneration and functional recovery[14]. Unlike EVLP systems, cross-circulation provides extracorporeal lungs with complete systemic support, including hepatic, pancreatic, renal and neurohormonal regulation, thereby enabling robust maintenance of healthy lungs outside the body for 4 d[15].

In this study, explanted human lungs declined for transplantation were supported using a cross-circulation platform. We hypothesized that 'xenogeneic' cross-circulation between explanted human lungs and a swine host could provide critical systemic regulation, maintain tissue structure and integrity and support functional lung recovery for 24 h. A regimen of immunosuppression drugs used in clinical lung transplantation was administered in combination with recombinant cobra venom factor to limit innate and adaptive immune responses. Throughout 24 h of xenogeneic

[1]Department of Biomedical Engineering, Columbia University, New York, NY, USA. [2]Department of Surgery, Columbia University Medical Center, Columbia University, New York, NY, USA. [3]Institute of Comparative Medicine, Columbia University Medical Center, Columbia University, New York, NY, USA. [4]Department of Thoracic Surgery, Vanderbilt University, Nashville, TN, USA. [5]Department of Clinical Perfusion, Columbia University Medical Center, Columbia University, New York, NY, USA. [6]Vagelos College of Physicians and Surgeons, Columbia University Medical Center, Columbia University, New York, NY, USA. [7]Department of Biomedical Engineering, Stevens Institute of Technology, Hoboken, NJ, USA. [8]Department of Medicine, Columbia University Medical Center, Columbia University, New York, NY, USA. [9]Department of Microbiology and Immunology, Columbia University Medical Center, Columbia University, New York, NY, USA. [10]Columbia Center for Human Development, Columbia University Medical Center, Columbia University, New York, NY, USA. [11]Department of Medicine, University of Southern California, Los Angeles, CA, USA. [12]Department of Stem Cell Biology and Regenerative Medicine, University of Southern California, Los Angeles, CA, USA. [13]Department of Pathology and Cell Biology, Columbia University Medical Center, Columbia University, New York, NY, USA. [14]Center for Translational Immunology, Columbia University Medical Center, Columbia University, New York, NY, USA. [15]Department of Cardiothoracic Surgery, Stanford University, Stanford, CA, USA. [16]Department of Cardiac Surgery, Vanderbilt University, Nashville, TN, USA. [17]Department of Biomedical Engineering, Vanderbilt University, Nashville, TN, USA. [18]Present address: Departments of Thoracic Surgery and Cardiac Surgery, Vanderbilt University, Nashville, TN, USA. [19]These authors contributed equally: Ahmed E. Hozain, John D. O'Neill, Matthew Bacchetta, Gordana Vunjak-Novakovic. ✉e-mail: matthew.bacchetta@vumc.org; gv2131@columbia.edu

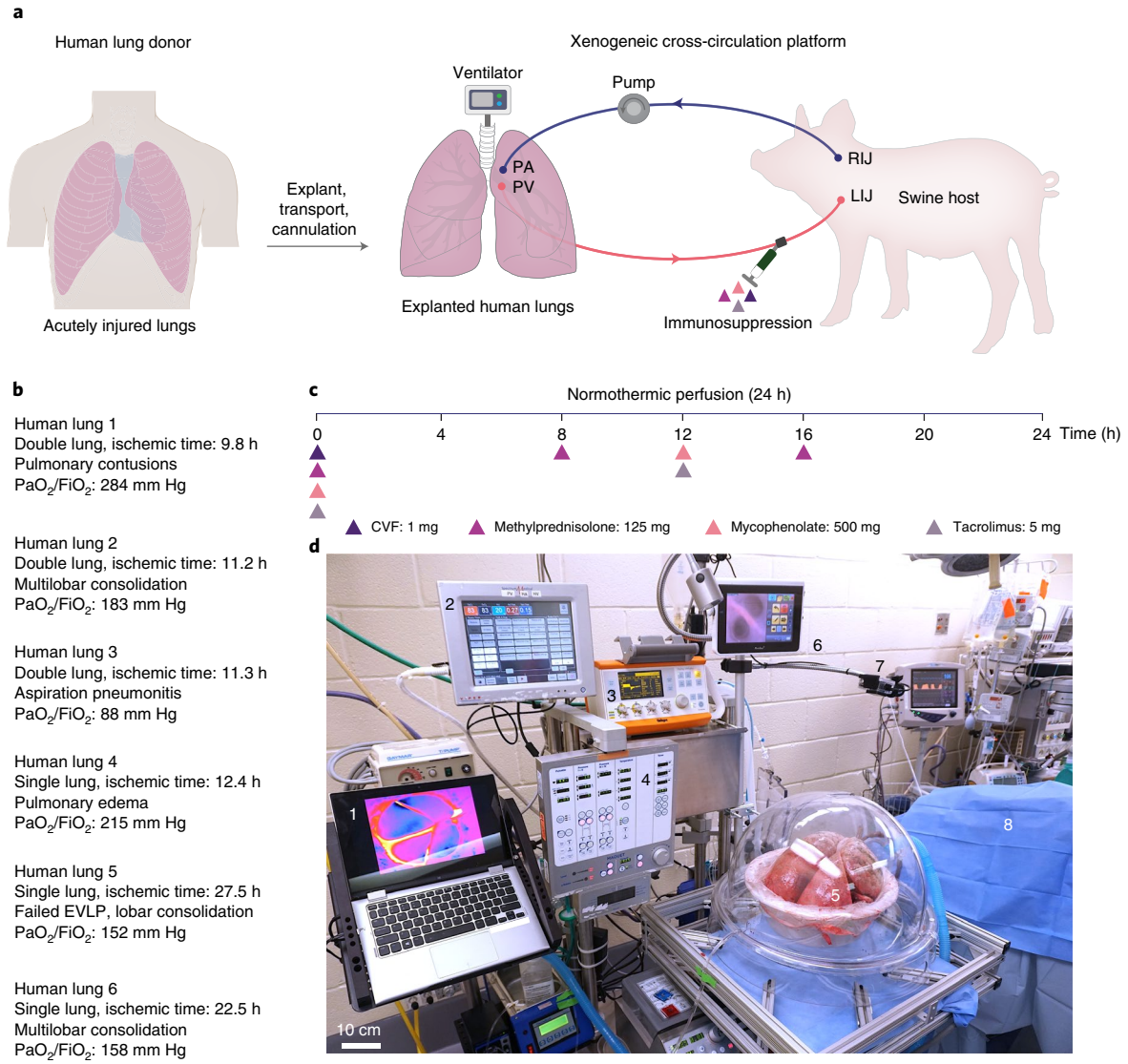

Fig. 1 | Maintenance of explanted human lungs using a xenogeneic cross-circulation platform. a, Human lungs deemed unsuitable for transplantation were procured in standard fashion, transported to the site of experimentation, and cannulated before initiation of cross-circulation with a swine host that was treated with an immunosuppression regimen. LIJ, left internal jugular vein; PA, pulmonary artery; PV, pulmonary vein; RIJ, right internal jugular vein. **b**, Characteristics of the six human lungs at initiation of xenogeneic cross-circulation. **c**, Experimental timeline for administration of the immunosuppression regimen over the course of 24 h of normothermic xenogeneic cross-circulation. The induction immunosuppression regimen administered before initiation of cross-circulation is described in Extended Data Fig. 1. **d**, Experimental setup for xenogeneic cross-circulation procedures. CVF, cobra venom factor. 1, thermography; 2, perfusion data acquisition system; 3, ventilator; 4, perfusion data display; 5, explanted human lungs; 6, video bronchoscopy; 7, time-lapse photography; 8, swine host.

cross-circulation, human lungs were subjected to multiscale longitudinal analyses of: (1) physiological and biochemical parameters; (2) respiratory function and lung histomorphology; (3) immunological activity and inflammatory response; and (4) cellular viability, phenotype and function.

Results

Characterization of xenogeneic cross-circulation system. A circuit to perfuse explanted human lungs was established with components routinely used for clinical perfusion: polyvinyl chloride flexible tubing, tubing connectors and a centrifugal pump. A swine host was anesthetized, cannulated through the internal jugular veins and connected to the circuit as previously described[10,14,15]. Explanted human lungs were connected to the circuit, marking the start of xenogeneic cross-circulation (Fig. 1a and Supplementary Video 1). Clinical characteristics of human lung donors are in Table 1. Human lungs were declined for transplantation due to pulmonary contusions with extensive multilobar hemorrhage (lung 1), pulmonary consolidation and edema (lungs 2–6) and aspiration pneumonitis with parenchymal opacities (lung 3; Fig. 1b). Notably, lung 5 was procured for xenogeneic cross-circulation after failure to recover during clinical EVLP.

As an immunological control, xenogeneic cross-circulation of explanted human lungs was performed without immunosuppression ($n=1$), which rapidly led to hemodynamic instability, significant increases in serum and airway inflammatory cytokines, pulmonary edema, diffuse alveolar hemorrhage, decreased respiratory function, thrombosis and irreversible graft dysfunction,

Table 1 | Demographics and clinical characteristics of human lung donors

Characteristics	Donor 1	Donor 2	Donor 3	Donor 4	Donor 5	Donor 6[a]
Age (years)	32	25	45	18	41	25
Sex	Male	Female	Female	Male	Male	Male
Cause of brain death	Trauma	Drug intoxication	Hemorrhagic stroke	Head trauma	Drug intoxication	Anoxia
Underlying lung disease	None	Asthma	Interstitial process	Asthma	None	None
Smoking history (pack-years)	7.5	4.5	8	0	20	0
Chest radiograph	Bilateral, multifocal pulmonary contusions	Right lower lobe atelectasis, consolidation	Left pleural effusion, atelectasis	Left apical pneumothorax	Right lower lobe infiltrates	Bilateral, patchy infiltrates
Time on ventilator (h)	83.4	137.6	192.1	60.5	223.7	239.5
Time from brain death to procurement (h)	69.3	66.2	12.7	48.5	–	–
PaO_2/FiO_2 at time of explant (mm Hg)[b]	400.2	250.5	280.1	407.6	410.0	113.5
Gram stain/BAL fluid culture	Gram-positive cocci	N/A	Gram-positive cocci, Gram-negative rods	None	*Enterobacter cloacae, Hafnia alvei*	*Staphylococcus aureus*
Single or double lung	Double	Double	Double	Single	Single	Single
Donation status	DBD	DBD	DBD	DBD	DCD	DCD
Clinical EVLP before xenogeneic XC (h)	0	0	0	0	5[c]	0
PaO_2/FiO_2 at end of EVLP	–	–	–	–	310	–

[a]Immunological control without immunosuppression. [b]FiO_2: 100%. [c]Reason lung declined for clinical transplantation after EVLP: right lower lobe failed to recruit. DBD, donation after brain death. DCD, donation after cardiac death.

consistent with hyperacute rejection (Supplementary Fig. 1). A regimen of immunosuppression drugs used for clinical lung transplantation in combination with recombinant cobra venom factor (a protein derived from cobra venom that depletes complement activity; Fig. 1c and Extended Data Fig. 1b) prevented acute rejection and enabled robust maintenance of explanted human lungs ($n=5$) throughout 24 h of xenogeneic cross-circulation (Fig. 1d).

A perfusion and ventilation strategy previously shown to preserve the structural and functional integrity of explanted lungs was implemented[14]. Throughout all procedures, mean pressure at the pulmonary artery was 15.7 ± 4.7 mm Hg, while mean pressure at the pulmonary veins was 3.4 ± 2.0 mm Hg. During normothermic perfusion (mean perfusate temperature: 35.4 ± 0.2 °C), flow rates in the pulmonary artery and veins matched (Extended Data Fig. 1a,g–i). Swine hosts remained hemodynamically and biochemically stable (mean heart rate, 102 ± 2 beats min^{-1}; systolic blood pressure, 88 ± 3 mm Hg; pH 7.43 ± 0.04; lactate; 1.6 ± 0.09 mmol l^{-1}) throughout 24 h of xenogeneic cross-circulation (Supplementary Table 1) and swine host organs had normal histomorphology after 24 h of xenogeneic cross-circulation (Supplementary Fig. 2).

Functional maintenance of explanted human lungs. Functional parameters are reported both as mean values ± s.d. for all lungs (Fig. 2) and as separate values for each set of lungs (Extended Data Figs. 2d–k, 3d–k, 4d–k, 5d–k and 6d–k). After 24 h of xenogeneic cross-circulation, human lungs with fraction of inspired oxygen (FiO_2) of 40% had a mean PaO_2/FiO_2 value of 320 ± 124 mm Hg, corresponding to a mean increase from baseline of 135 mm Hg (Fig. 2a). Mean dynamic compliance was maintained at 15–45 ml cmH_2O^{-1} and consistently increased throughout 24 h of xenogeneic cross-circulation (Fig. 2b). Oxygenation and ventilation were assessed by differences (Δ) in the partial pressures of hemogases at the inflow (pulmonary artery) and outflow (pulmonary veins) of the lungs (Extended Data Fig. 1a). Mean oxygenation (ΔpO_2) and ventilation (ΔpCO_2) steadily increased over 24 h (Fig. 2c). Peak inspiratory pressures decreased over 24 h of xenogeneic cross-circulation, from 19.4 ± 6.7 cmH_2O to 15.6 ± 5.8 cmH_2O, whereas mean airway pressures were maintained at 8.5 ± 2.4 cmH_2O (Fig. 2d). Notably, after 24 h of xenogeneic cross-circulation, all lungs ventilated at the target tidal volume of 6 ml kg^{-1} showed improved recruitment (Supplementary Video 2) consistent with improvements in functional parameters.

Lung weight, an indicator of pulmonary vascular integrity[16], did not increase from baseline after 24 h of xenogeneic cross-circulation (Fig. 2e). Transpulmonary pressure gradient, a measure of pulmonary vascular resistance, was maintained within the target range of 5–15 mm Hg (Fig. 2f) and mean lactate level at the pulmonary veins remained below 3 mmol l^{-1} (Fig. 2g). Throughout all procedures, pH was maintained at 7.43 ± 0.04 (Fig. 2h). Overall, mean changes in functional parameters over 24 h confirmed that the xenogeneic cross-circulation platform supported recovery of human lung respiratory function: mean PaO_2/FiO_2 increased by 117%, mean dynamic compliance increased by 185% (Fig. 2i) and mean peak inspiratory pressure decreased by 16%, with minimal changes in lung weight, transpulmonary pressure gradient and lactate (Fig. 2j).

Multiscale analyses of explanted human lungs. Lung integrity is reported by representative images and mean values ± s.d. for all lungs (Fig. 3) and individual images and values for each set of lungs (Extended Data Figs. 2a–c, 3a–c, 4a–c, 5a,b and 6a,b). Gross appearance of human lungs at initiation of xenogeneic cross-circulation revealed varying but extensive consolidation, pulmonary edema and hemorrhage. After 24 h, lungs showed reduced consolidation and improved aeration (Fig. 3a). Radiography enabled periodic noninvasive assessment of each lobe and revealed focal and diffuse consolidations before xenogeneic cross-circulation. Progressive clearance of regional consolidation was observed after 24 h, with increased radiolucency and extensive recovery of ventilating lung

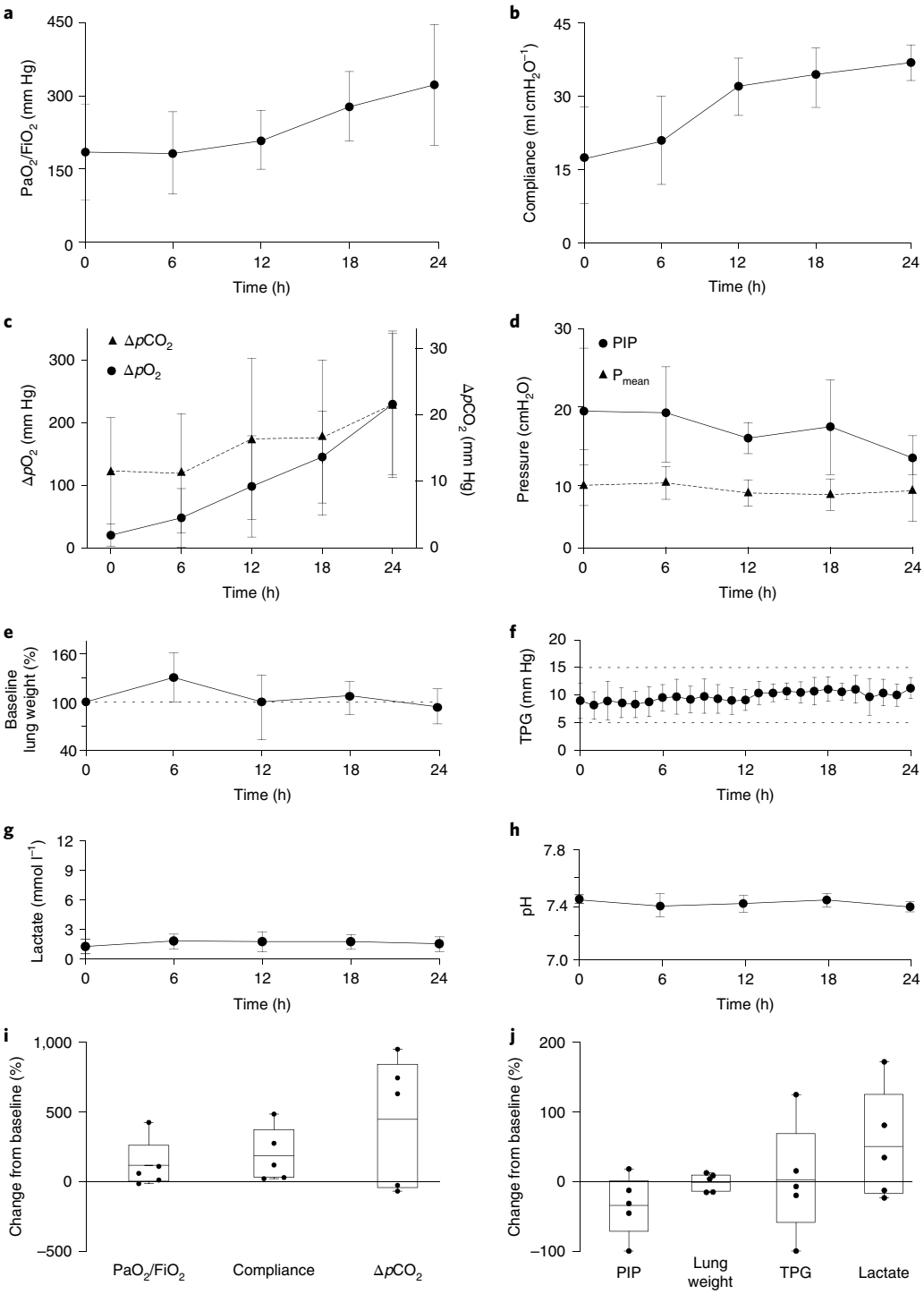

Fig. 2 | Human lung function over the course of 24 h of xenogeneic cross-circulation. a, PaO_2/FiO_2. **b**, Dynamic compliance. **c**, Changes in pO_2 and pCO_2 ($\Delta p = |p_{PA} - p_{PV}|$). **d**, Peak inspiratory pressure (PIP) and mean airway pressure (P_{mean}). **e**, Lung weight. **f**, Transpulmonary pressure gradient (TPG), defined as the vascular pressure difference between the pulmonary artery and pulmonary vein. **g**, Lactate concentrations. **h**, pH. **i**,**j**, Changes in physiological and functional parameters between baseline and after 24 h of xenogeneic cross-circulation. All graphs represent data for human lungs ($n = 5$ independent experiments). Box-and-whisker plots show lower and upper quartiles, the center line represents the mean of each sample group, the vertical lines represent the maximum and minimum, and the dots represent each human lung. All line graph values represent mean ± s.d.

volume (Fig. 3b). Before xenogeneic cross-circulation, video bronchoscopy revealed mild secretions with airway inflammation. However, by 12 h, large airways seemed normal without evidence of airway secretions, edema or erythema (Fig. 3c).

Histological analyses confirmed maintenance of conducting airway structures, including intact pseudostratified epithelium in segmental and subsegmental bronchi after 24 h of xenogeneic cross-circulation (Fig. 3d and Extended Data Figs. 7c, 8c and 9c). Edema, intimal thickening and cellular derangement in lung parenchyma were minimal (Fig. 3e and Extended Data Figs. 5c, 6c, 7a,b,d, 8a,b,d and 9a,b,d) and extensive alveolar recruitment and aeration were consistent with diagnostic radiography. Scanning electron

microscopy revealed that alveolar architecture was initially perturbed, with vascular exudate and/or alveolar hemorrhage. After 24 h, alveolar architecture seemed substantially restored, with minimal evidence of extravasation or structural degradation (Fig. 3f and Extended Data Figs. 7e, 8e and 9e). Transmission electron microscopy enabled detailed assessment of the alveolar–capillary barrier, which seemed damaged or disrupted before initiation of xenogeneic cross-circulation, but nevertheless retained the blood–gas interface throughout 24 h (Fig. 3g and Extended Data Figs. 7f, 8f and 9f).

Histopathology and airway inflammatory response. Lung injury was evaluated by blinded histopathological assessment, which included quantification of airway and alveolar polymorphonuclear cells, alveolar and interstitial edema, interstitial infiltrate and early (caspase 3^+) and late ($TUNEL^+$) apoptotic cells (Supplementary Table 2). Injury scores at 0, 12 and 24 h of xenogeneic cross-circulation decreased from baseline across multiple lung injury categories (Fig. 3h and Supplementary Fig. 3). Although the alveolar and interstitial edema combined score increased slightly above baseline (0 h, 0.44; 24 h, 0.69), the early and late apoptosis combined score decreased by 63.6% (0 h, 2.26; 24 h, 0.82). The airway and alveolar polymorphonuclear cells combined score decreased by 51.7% (0 h, 1.09; 24 h, 0.53) and the composite lung injury score decreased by 45.1% (0 h, 5.04 ± 0.70; 24 h, 2.76 ± 0.65) over 24 h of xenogeneic cross-circulation (Fig. 3i).

Inflammation of pulmonary airways was assessed by analyses of bronchoalveolar lavage (BAL) fluid, including staining of BAL fluid smears and quantification of airway inflammatory cytokines. At initiation of xenogeneic cross-circulation, BAL fluid samples seemed reddish and turbid, suggesting the presence of blood, mucus and cellular debris. After 24 h, with periodic airway lavage, BAL fluid seemed clear, consistent with cytological smears that showed reduced cellular debris between 0 h and 12 h and normal pH 5.5 by 24 h (Fig. 3j). In BAL fluid, total protein concentration, a measure of airway secretions and leakage of serum proteins across the epithelial barrier, remained constant throughout 24 h, suggesting no degradation of the blood–gas barrier (Fig. 3k). Mean concentrations of inflammatory cytokines interferon (IFN)-γ, interleukin (IL)-1α, IL-1β, IL-1ra, IL-2, IL-8, IL-12, IL-16, 1L-17a, IL-18, tumor necrosis factor (TNF)-α and TNF-β decreased in BAL fluid, whereas mean concentrations of IL-4, IL-5, IL-6 and IL-10 increased (Fig. 3l and Supplementary Tables 3–7). Notably, in BAL fluid the only statistically significant increase in mean cytokine concentration was IL-6 (4.7-fold), whereas mean concentrations of IL-1β, IL-1ra and IL-18 significantly decreased (9.5-, 5.4- and 2.7-fold, respectively). To assess microbial burden, cultures from BAL fluid samples were qualitatively analyzed for bacterial and fungal growth at baseline and 24 h (Supplementary Table 8).

Pulmonary endovascular integrity and immune responses. Endothelial cells are the first to interact with nonself antigens in organ transplantation and serve as key regulators of immune response and coagulation. After 24 h of xenogeneic cross-circulation, angiography confirmed patency and preservation of the pulmonary vascular tree throughout all lobes and peripheral regions (Fig. 4a). Pentachrome staining revealed that endothelial surfaces of large pulmonary arteries and veins were free of fibrin deposition, and elastic fibers in arterial and venous vessel walls retained stereotypical organization and distribution (Fig. 4b). Arterioles and venules retained normal endothelial cell morphology (Fig. 4c). Transmission electron microscopy of pulmonary capillaries confirmed retention of intact alveolar–capillary barrier without evidence of microthrombi (Fig. 4d).

After 24 h of xenogeneic cross-circulation, complete blood count and immunostaining for clotting (fibrin) and platelet activation (glycoprotein IIb/IIIa) markers showed no evidence of thrombotic deposition in large vessels (Fig. 4e) or thrombocytopenia (Fig. 4f). Mean hematocrit was consistently maintained above 28% (Supplementary Table 1), indicating minimal hemolysis. Markers of platelet activation, including fibrinogen (clotting precursor), D-dimer (fibrin degradation product) and plasma-free hemoglobin (hemolysis marker) remained within normal ranges (Fig. 4g). Remarkably, P-selectin, a marker of endothelial injury and platelet/leukocyte activation, decreased from 22.8 ng ml^{-1} to 4.9 ng ml^{-1} (Fig. 4g). Altogether, human lungs on xenogeneic cross-circulation retained integrity of the delicate pulmonary vascular endothelium without evidence of significant injury, activation or thrombotic microangiopathy associated with acute immunologic rejection.

Viability and phenotypic maintenance of pulmonary vascular endothelial cells were confirmed, respectively, after 24 h by pervasive uptake of cell viability marker carboxyfluorescein succinimidyl ester (CFSE) (Fig. 4h) and normal distribution of vascular endothelial (VE)-cadherin (Fig. 4i). Uptake of acetylated low-density lipoprotein confirmed endothelial cell function in small and large vessels (Fig. 4j). Immunostaining for α-smooth muscle actin (α-SMA) indicated myocyte preservation in pulmonary vascular smooth muscle (Fig. 4k), which displayed an expected increase in arterial pressure after intravascular injection of phenylephrine (Fig. 4l). To assess transcriptomic changes in endothelial-associated genes, differential gene expression analysis was performed between 0 and 24 h and compared to expression in normal human lungs from the Genotype-Tissue Expression Consortium. Throughout xenogeneic cross-circulation, explanted human lungs demonstrated no statistically significant difference in expression of 19 endothelial-associated genes across time points or compared to normal lungs (Fig. 4m, Supplementary Fig. 4a,c and Supplementary Data 1), suggesting that endothelial cell phenotype was not significantly altered during xenogeneic cross-circulation.

Serum cytokines serve as major regulators of immune response after organ transplantation. Quantification by multiplex array of circulating swine cytokines revealed that from baseline to 24 h, concentrations of IL-1α, IL-1β, IL-1ra, IL-2, IL-4, IL-6, IL-8, IL-10, IL-12 and IL-18 changed minimally between −2.9-fold and +5.3-fold (Fig. 4n and Supplementary Table 9). Fold change increases in serum concentrations were greatest for IFN-γ (+76.8),

Fig. 3 | Multiscale analyses of human lungs over the course of 24 h of xenogeneic cross-circulation. a–c, Gross appearance (**a**), radiographs (**b**) and bronchographs (**c**) of representative lungs. **d**,**e**, Hematoxylin and eosin staining of small airways (**d**) and lung parenchyma (**e**). **f**, Scanning electron microscopy for visualization of alveolar structure. **g**, Transmission electron microscopy for visualization of the alveolar–capillary barrier. **h**, Histopathologic lung injury scores visualized using a radar plot. Injury score aligned to the vertical axis represents injury score in seven measured parameters. Each overlaid radar plot represents an individual time point ($n = 5$ independent experiments). Asterisks represent statistical significance: caspase 3, $P < 0.0001$; interstitial infiltrate $P < 0.0023$. PMN, polymorphonuclear cells. **i**, Composite lung injury scores. **j**, Representative images of periodic acid-Schiff staining of BAL fluid smears. Inset: gross images of BAL fluid from human lung 1. **k**, Quantification of total protein in BAL fluid ($n = 3$ independent experiments). **l**, Quantification of inflammatory cytokines in BAL fluid ($n = 5$ independent experiments). Asterisks represent statistical significance: IL-1β, $P = 0.0197$; IL-1ra, $P = 0.0054$; IL-18, $P = 0.0129$; IL-6, $P < 0.0001$. All images are representative of human lungs from one donor. All values represent mean values or mean ± s.d. Representative images of human lungs 1–5 are shown in Extended Data Figs. 2–9. Quantification of cytokines in BAL fluid from human lungs 1–5 is shown in Supplementary Tables 3–7. Lung injury scores for human lungs 1–3 are shown in Supplementary Fig. 3. One-way ANOVA (**h**) and paired Student's *t*-test (**l**) were used to determine statistical significance.

TNF-α (+23.5), granulocyte–macrophage colony-stimulating factor (+7.5) and IL-1ra (+5.3), although only TNF-α and IL-12 had statistically significant changes between baseline and 24 h.

Innate immune activity was assessed by total complement activity (CH50) assay, which confirmed depletion of complement activity before the start of xenogeneic cross-circulation (Fig. 4o). Without

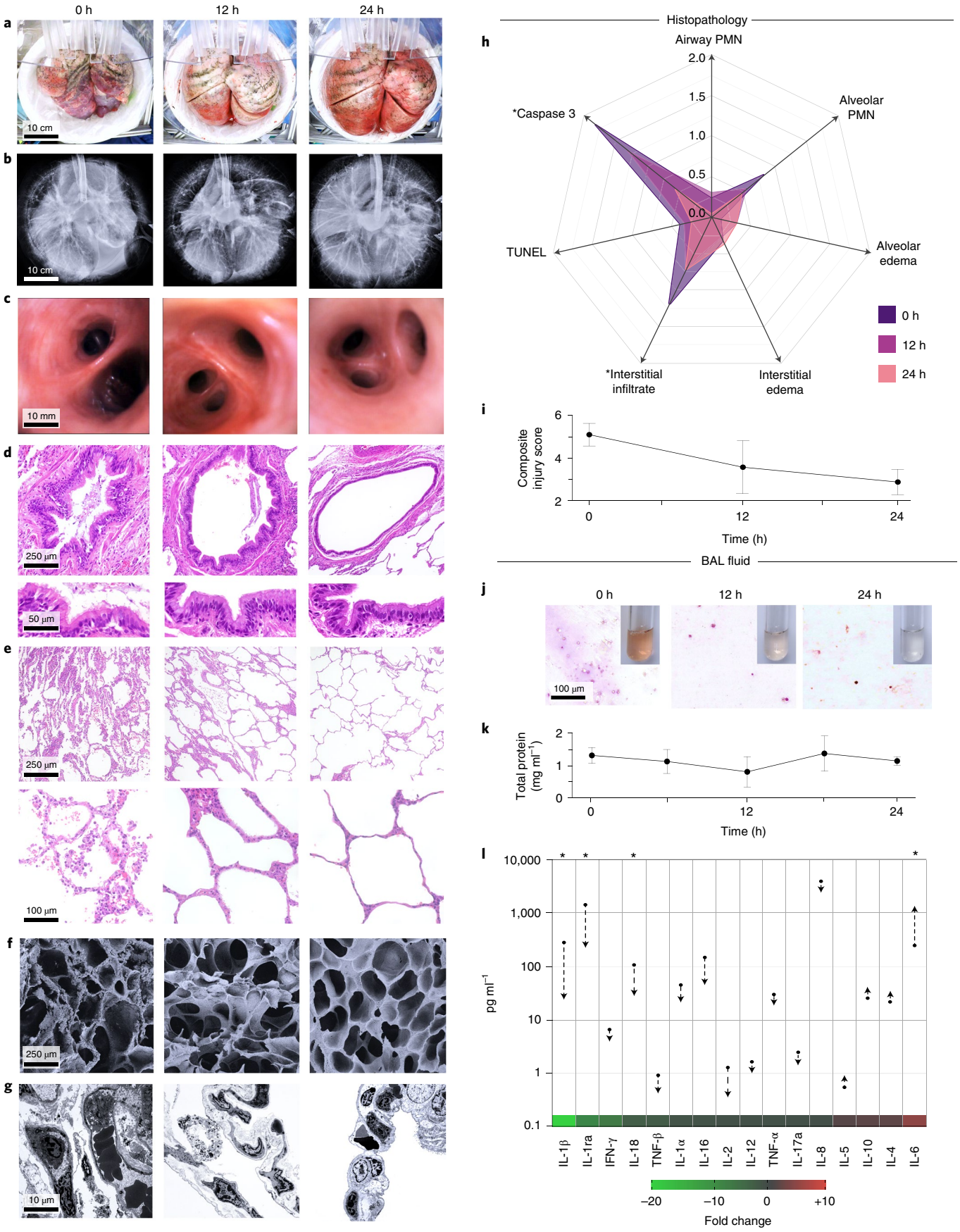

immunosuppression, complement components C3b and C5b-9 demonstrated deposition throughout lung tissue within 30 min of initiating xenogeneic cross-circulation (Supplementary Fig. 1o,p). Suppression of cell-mediated immune response was achieved by therapeutic doses of methylprednisolone, mycophenolate and tacrolimus (FK506; Supplementary Table 1).

To assess retention of leukocytes in human lungs, CD45$^+$ leukocytes were quantified by immunostaining for swine galactose-α-1,3-galactose (α-Gal) and human nuclear antigen (HNA). Representative images revealed the presence of human (HNA$^+$) leukocytes after 24 h (Fig. 4p), although quantitative analysis indicated progressive clearance of human CD45$^+$ leukocytes from the lungs over 24 h of xenogeneic cross-circulation. After an initial increase at the start of cross-circulation, swine CD45$^+$ leukocytes in human lungs also decreased over 24 h (Fig. 4q). Neutrophils (human and swine), responders to ischemia–reperfusion injury and acute inflammation were initially elevated, but by 12 h were drastically reduced in alveolar and interstitial compartments (Fig. 4r). Similarly, CD163$^+$ macrophages (human and swine), key regulators of immune response, were initially more abundant in alveolar spaces, likely in response to donor injuries, but by 24 h were reduced. The number of CD163$^+$ macrophages in the interstitium remained constant across 24 h of xenogeneic cross-circulation (Fig. 4s).

Cellular integrity, phenotype and function. After 24 h of xenogeneic cross-circulation, lung regions that had been initially consolidated were recruited (Fig. 5a). Pentachrome staining confirmed outstanding maintenance of gross structure in main and lobar bronchi (Fig. 5b). Pseudostratified airway epithelium with mucus-containing goblet cells (Fig. 5c) and ciliated airway epithelial cells with intact ciliated brush border (Fig. 5d) were observed throughout large airways. Histomorphology of airway secretory glands (Fig. 5e) and airway smooth muscle myocytes (Fig. 5f) seemed normal. Notably, regenerative airway stem cell populations, including p63$^+$ basal cells (Fig. 5g) and α-SMA$^+$ submucosal gland epithelial cells (Fig. 5h) observed at baseline, were retained after 24 h (Extended Data Fig. 7k,l), suggesting that the potential for endogenous repair of airways was preserved through xenogeneic cross-circulation.

To assess the structural integrity of small airways in explanted human lungs, airway casts were prepared and confirmed maintenance of bronchiolar architecture and respiratory bronchioles (Fig. 5i). Immunostaining for epithelial cell adhesion molecule (EpCAM) revealed undisrupted columnar respiratory epithelium with intact underlying airway smooth muscle (Fig. 5j), which was responsive after 24 h of xenogeneic cross-circulation to nebulized administration of bronchomotor regulatory agents (Fig. 5k). Primary respiratory epithelial cell phenotypes were preserved throughout small airways, including ciliated cells (Fig. 5l), club cells (Fig. 5m), neuroendocrine cells (Fig. 5n) and goblet cells (Fig. 5o). Ubiquitous uptake of viability marker CFSE in distal lung regions confirmed parenchymal cell viability (Fig. 5p), and mitochondrial activity assay indicated that explanted human lungs maintained constant metabolic activity throughout 24 h of xenogeneic cross-circulation (Fig. 5q).

Expression of genes associated with pulmonary epithelium was assessed by RNA sequencing, which revealed no significant difference in expression of 27 epithelial-associated genes across time points or compared to normal human lungs (Fig. 5r, Supplementary Fig. 4b,c and Supplementary Data 1). Pulmonary microvascular CD31$^+$ endothelial cells exhibited typical colocalization with tight junction protein ZO-1 (Fig. 5s), confirming retention of tight junctions in the pulmonary capillary plexus. Pericytes, critical support cells for alveolar capillaries, were also maintained throughout the distal lung (Fig. 5t). Type I pneumocytes were visualized by aquaporin 5 (Fig. 5u) and caveolin-1 (Fig. 5v) amid normal distribution of epithelial tight junction protein ZO-3 (Fig. 5w), consistent with lung weight and electron microscopy that confirmed maintenance of respiratory epithelium in distal lung regions after 24 h. Type II pneumocytes retained expression of HT2-280 (Fig. 5x) and surfactant protein C (Fig. 5y) and internalized fluorescently labeled surfactant protein B (SPB-BODIPY; Fig. 5z and Supplementary Video 3), confirming viability and uptake function of type II cells after 24 h of xenogeneic cross-circulation. Additional representative micrographs of human lungs at baseline and 24 h of xenogeneic cross-circulation are in Extended Data Figs. 7g–n, 8g–l and 9g–l.

Discussion

We describe a xenogeneic cross-circulation system that supports the viability and functional recovery of human donor lungs declined for transplantation. Despite compromised respiratory function ($PaO_2/FiO_2 < 300$ mm Hg) at baseline due to common injury etiologies, including (1) traumatic lung injury (lung 1), (2) severe pulmonary consolidation and edema (lungs 2, 4 and 5) and (3) aspiration pneumonitis (lung 3), human lungs consistently demonstrated functional and histological improvements throughout 24 h of xenogeneic cross-circulation.

Notably, we also show that cross-circulation recovered a lung that failed clinical EVLP (lung 5). After procurement (cold ischemia time no. 1: 2.3 h), bilateral lungs were placed on clinical EVLP

Fig. 4 | Endovascular integrity and immunologic response over the course of xenogeneic cross-circulation. a–d, Characterization of the pulmonary vasculature in lungs at 24 h of xenogeneic cross-circulation, as assessed by angiogram demonstrating patent pulmonary vasculature (**a**); pentachrome staining (**b**); hematoxylin and eosin staining (**c**); and transmission electron microscopy demonstrating intact alveolar–capillary barrier (pseudocolored), red blood cells (red), endothelial cell membrane (blue) and endothelial cell nucleus (orange) (**d**). **e**, Immunohistochemical staining of fibrin and glycoprotein IIb/IIIa (GpIIb/IIIa), showing lack of thrombus deposition in large vessels identified by VE-cadherin staining after 24 h. Asterisk indicates vessel lumen. Positive control staining performed on a thrombus formed on a glass slide (insets). **f**,**g**, Quantification of platelets (**f**) and hemolytic and injury markers (**g**) ($n = 3$ independent experiments). Hgb, hemoglobin. **h–k**, Characterization of the pulmonary endothelium in lungs at 24 h of xenogeneic cross-circulation. Staining for uptake of the cell viability marker CFSE (**h**). Asterisk indicates vessel lumen. Immunohistochemical staining for the endothelial cell marker VE-cadherin (**i**). Staining for uptake of acetylated low-density lipoprotein (aLDL) (**j**). Immunohistochemical staining for the vascular smooth muscle cell marker α-SMA (**k**). **l**, Vasoresponsiveness of pulmonary vasculature to phenylephrine after 24 h of xenogeneic cross-circulation ($n = 1$ independent experiment). **m**, Relative expression of 19 endothelial-associated genes in human lungs at 0 h ($n = 2$ lung tissue replicates) and 24 h ($n = 3$ lung tissue replicates) of xenogeneic cross-circulation, compared to normal human lungs ($n = 50$ random samples) from the Genotype-Tissue Expression database. **n**, Quantification of serum cytokines ($n = 3$ independent experiments). **o**, Quantification of complement activity (CH50) after administration of CVF 4 h before initiation of xenogeneic cross-circulation (XC) ($n = 3$ independent experiments). **p**, Immunohistochemical staining of swine and human CD45$^+$ leukocyte deposition in human lung tissue over the course of xenogeneic cross-circulation. **q–s**, Quantification of swine and human CD45$^+$ leukocytes (**q**), neutrophil elastase$^+$ cells in alveolar and interstitial spaces (**r**), and CD163$^+$ cells in alveolar and interstitial spaces (**s**) ($n = 3$ independent experiments). hpf, high-powered field. All images are representative of human lungs from one donor; **a–e**,**h–k** represent data after 24 h of xenogeneic cross-circulation. All values represent mean values or mean ± s.d. Box-and-whisker plot shows lower and upper quartile values, center line represents the median of each sample group, vertical lines represent maximum and minimum values, and dots represent outliers from sample groups.

for 5 h. After EVLP, the left lung was allocated for transplantation. However, the right lung (lung 5) demonstrated persistent lobar consolidation and was declined for transplantation by multiple transplant centers. Subsequently, lung 5 was offered for research, transported to the site of cross-circulation (cold ischemia time no. 2: 19.2 h) and placed on xenogeneic cross-circulation. Thus, before xenogeneic cross-circulation, lung 5 suffered two periods of cold ischemia (total: 22.5 h) interspersed by 5 h of normothermic EVLP, conditions known to induce ischemia–reperfusion injury leading to reduced lung integrity and function[17]. Nevertheless, after 24 h of xenogeneic cross-circulation, lung 5 showed reduced consolidation, successful recruitment of the lower lobe and functional and

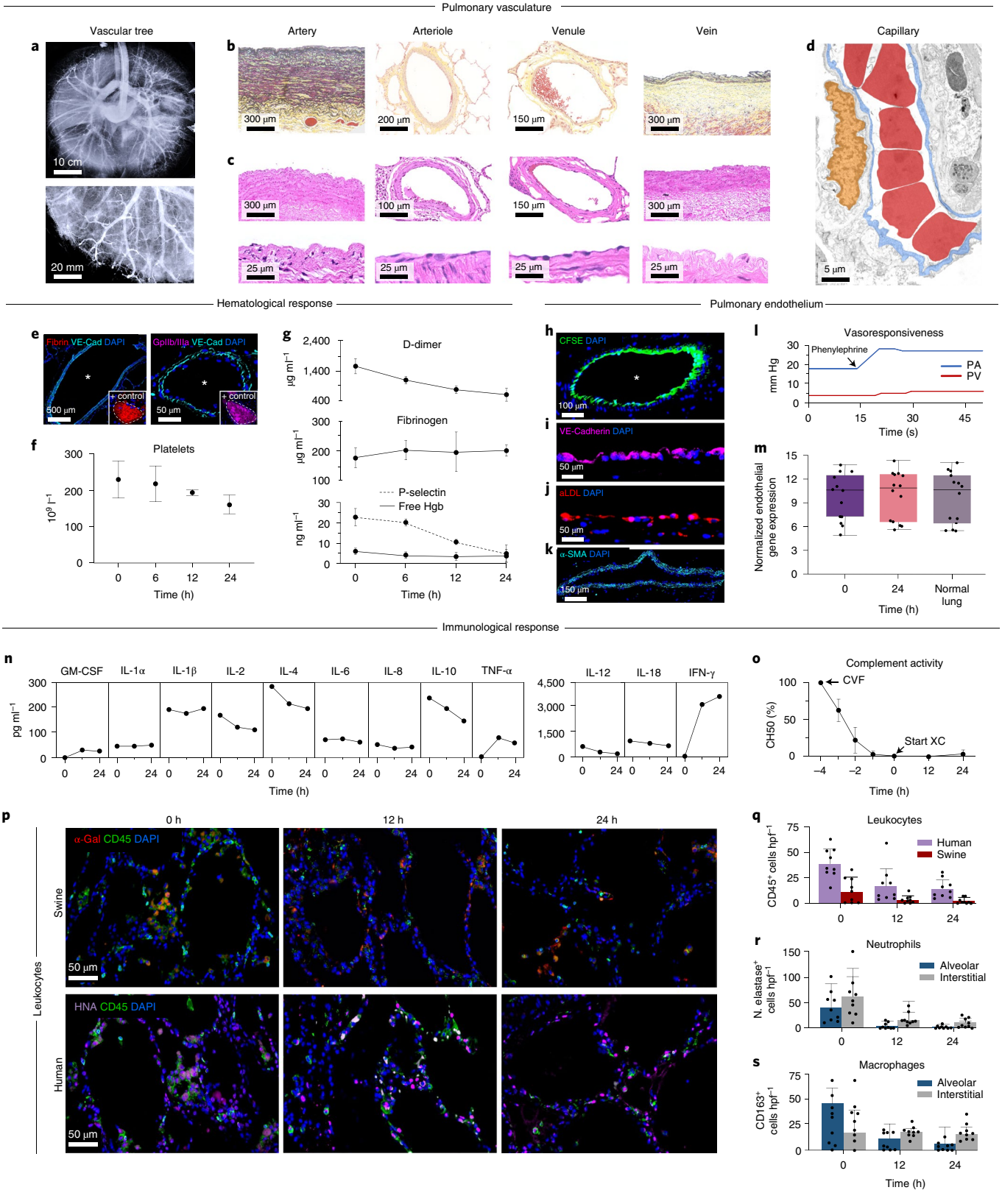

histological improvements (Supplementary Table 10). These results suggest that cross-circulation could be developed as a complementary approach for lungs that standard EVLP cannot recover.

Lungs in this study were severely injured and subjected to long cold ischemia times before extracorporeal support, yet after 24 h of xenogeneic cross-circulation showed significant functional improvements (Supplementary Table 11) and lower concentrations of inflammatory cytokines (Supplementary Table 12) than previously reported[9,18–23]. Except for slight increases in edema (likely due to the static prone positioning of lungs throughout cross-circulation), histopathological injury scores steadily decreased throughout 24 h of xenogeneic cross-circulation and approached those of transplanted human lungs in multiple categories. Previously, mechanisms of airway and alveolar repair after acute lung injury have been shown to involve proliferation and differentiation of endogenous lung progenitor cells (for example, differentiation of type II to type I pneumocytes to restore the alveolar epithelial barrier)[24]. Thus, retention of p63$^+$ airway basal cells[25], α-SMA$^+$ submucosal epithelial cells[26] and HT2-280$^+$ type II cells[27] after 24 h of xenogeneic cross-circulation suggests that multiple endogenous airway and alveolar progenitor cell populations critical for tissue regeneration were preserved from baseline. In the future, therapeutic strategies aimed at promoting endogenous repair could be employed during multiday cross-circulation to accelerate recovery of more lungs and expand the supply of available organs.

Research efforts in xenotransplantation have aimed to create an unlimited supply of swine organs for human transplantation.[8] Swine are extensively utilized in xenotransplantation research due to their physiological similarity to humans. Despite advances in genetically engineered swine to eliminate acute xenograft rejection, chronic xenoantigen exposure leading to antibody-mediated rejection and graft failure[28] remains problematic. Notably, xenogeneic cross-circulation could circumvent the translational barriers of xenotransplantation because: (1) during xenogeneic cross-circulation, human lung exposure to circulating swine xenoantigens is transient, mitigating risk of chronic rejection; and (2) human lungs recovered via xenogeneic cross-circulation would be used for allograft transplantation of a human organ into a human recipient, precluding risks associated with xenograft antibody-mediated rejection. Previously, patients on dialysis[29] and those with liver failure[30] who experienced acute exposure to swine xenoantigens developed anti-swine xenoantibodies, but subsequently underwent successful transplantation of kidney or liver allografts[31]. A review of eight studies investigating sensitization to swine antigens concluded that after sensitization to swine antigens, there was no evidence of antibody-mediated or accelerated cellular rejection of a subsequent allograft[32]. These findings suggest that a human organ transiently exposed to swine xenoantigens during xenogeneic cross-circulation could be tolerated by a transplant recipient.

To reduce risk of acute rejection during the procedure, an immunosuppression regimen informed by practices in clinical lung transplantation[33] was implemented: triple therapy of tacrolimus (calcineurin inhibitor), mycophenolate (antiproliferative agent) and methylprednisolone (corticosteroid), in combination with cobra venom factor (complement-activating protein that depletes complement activity[34]). Interestingly, cobra venom factor has been shown to eliminate acute xenograft rejection[35], preserve tight junction integrity[36] and decrease ischemia–reperfusion injury associated with transplantation[36,37]. Accordingly, after 24 h of xenogeneic cross-circulation, explanted human lungs demonstrated patent microvasculature, intact blood–gas barrier and decreased serum P-selectin, with no evidence of clotting or angiopathy.

In this study, an immunological control without immunosuppression (lung 6) resulted in severe immunological rejection within 1 h of xenogeneic cross-circulation, validating the need for an immunosuppressive regimen. We also report transcriptomic analyses of human lungs during xenogeneic cross-circulation and establish benchmarks of inflammatory cytokines in BAL fluid and serum. IL-1β and IL-8, markers of leukocyte infiltration[38,39] and primary graft dysfunction following lung transplantation[40,41], showed minimal changes from baseline in both BAL fluid and serum. While mean serum concentrations of IFN-γ and TNF-α increased, the only BAL fluid cytokine that demonstrated a statistically significant increase was IL-6, which has been reported to both have both pro- and anti-inflammatory activities[42]. Notably, IFN-γ has been shown to protect early graft survival[43]. Altogether, these findings suggest that after 24 h of xenogeneic cross-circulation with immunosuppression, human lungs experienced minimal endothelial activation[44] and immune response[45,46] and showed no clinical signs of acute rejection.

Future studies will assess the potential for clinical translation of xenogeneic cross-circulation. The experimental use of Yorkshire swine for xenogeneic cross-circulation resulted in the localization of swine cells (for example, α-Gal$^+$CD45$^+$ leukocytes) in human lungs, indicating a degree of human–swine chimerism. Although chimerism has been shown to induce graft tolerance[47], further characterization of the immunological mechanisms and residual swine antigens in lungs recovered by xenogeneic cross-circulation is needed. Before clinical translation, acceptable criteria for residual swine factors must be established. Evaluation of humanized swine[7,48], immunodeficient swine[49] and targeted lymphodepletion therapies[50–52] may inform strategies to limit maladaptive immune

Fig. 5 | Maintenance of pulmonary airways and alveolar–capillary barrier after 24 h of xenogeneic cross-circulation. a, Gross appearance of human lung 5, demonstrating right lower lobe recruitment (dashed lines). **b**–**f**, Pentachrome staining of large airway structures (**b**), goblet cells containing mucin (**c**), intact cilia (**d**), submucosal glands (**e**) and airway smooth muscle (**f**). **g**, Immunohistochemical staining for p63, identifying airway p63$^+$ basal cells. **h**, Airway submucosal glands identified by pentachrome staining, demonstrating central mucus stores (left), and by immunohistochemistry, demonstrating α-SMA$^+$ myoepithelial cells (right). **i**–**o**, Small airway structure and function. Polyurethane airway cast of preserved small airways and respiratory bronchioles (**i**). Immunohistochemical staining of small airway columnar epithelium (EpCAM) and smooth muscle (α-SMA) (**j**). Bronchoresponsiveness of airway smooth muscle to albuterol and methacholine ($n=1$ independent experiment) (**k**). Immunohistochemical staining for identification of α-tubulin$^+$ ciliated cells (**l**), CC10$^+$ club cells (**m**), PGP9.5$^+$ neuroendocrine cells (**n**) and mucin5B$^+$ goblet cells (**o**). **p**, Staining for uptake of viability marker CFSE by parenchymal cells. **q**, Quantification of lung cellular metabolic activity standardized to total sample DNA ($n=3$ independent experiments). **r**, Relative expression of 27 epithelial-associated genes in human lungs at 0 h ($n=2$ tissue replicates) and 24 h ($n=3$ tissue replicates) of xenogeneic cross-circulation, compared to normal human lungs ($n=50$ random samples) from the Genotype-Tissue Expression database. **s**–**y**, Maintenance of alveolar–capillary barrier as assessed by immunohistochemical staining for identification of CD31$^+$ endothelial cells and ZO-1$^+$ microvascular tight junctions (**s**), NG2$^+$ pericytes (**t**), Aqp5$^+$ type I pneumocytes (**u**), Cav-1$^+$ type I pneumocytes (**v**), ZO-3$^+$ epithelial tight junctions (**w**), HT2-280$^+$ type II pneumocytes (**x**) and SPC$^+$ type II pneumocytes (**y**). **z**, Staining for uptake of fluorescent BODIPY-SPB by live type II pneumocytes. Images are representative of human lungs from one donor. Dashed lines in **g**,**h**,**j**,**l**–**o** indicate airway basement membrane. Line graphs represent mean or mean ± s.d. Box-and-whisker plot shows lower and upper quartile values, center line represents the median of each sample group, vertical lines represent maximum and minimum values and dots represent outliers from sample groups. Aqp5, aquaporin 5; Cav-1, caveolin-1; NG2, neural/glial antigen 2; OD, optical density; PEEP, positive end-expiratory pressure; SPB, surfactant protein B; SPC, surfactant protein C; ZO-1, zonula occludens-1; ZO-3, zonula occludens-3.

responses and facilitate clinical translation. To reduce the risk of zoonotic disease transmission[53], medical-grade swine from designated pathogen-free barrier facilities[54] can be screened using PCR and next-generation sequencing methods[55,56]. Although porcine endogenous retrovirus (PERV) is carried in the swine genome and presents a unique infectious risk, swine genome editing has been

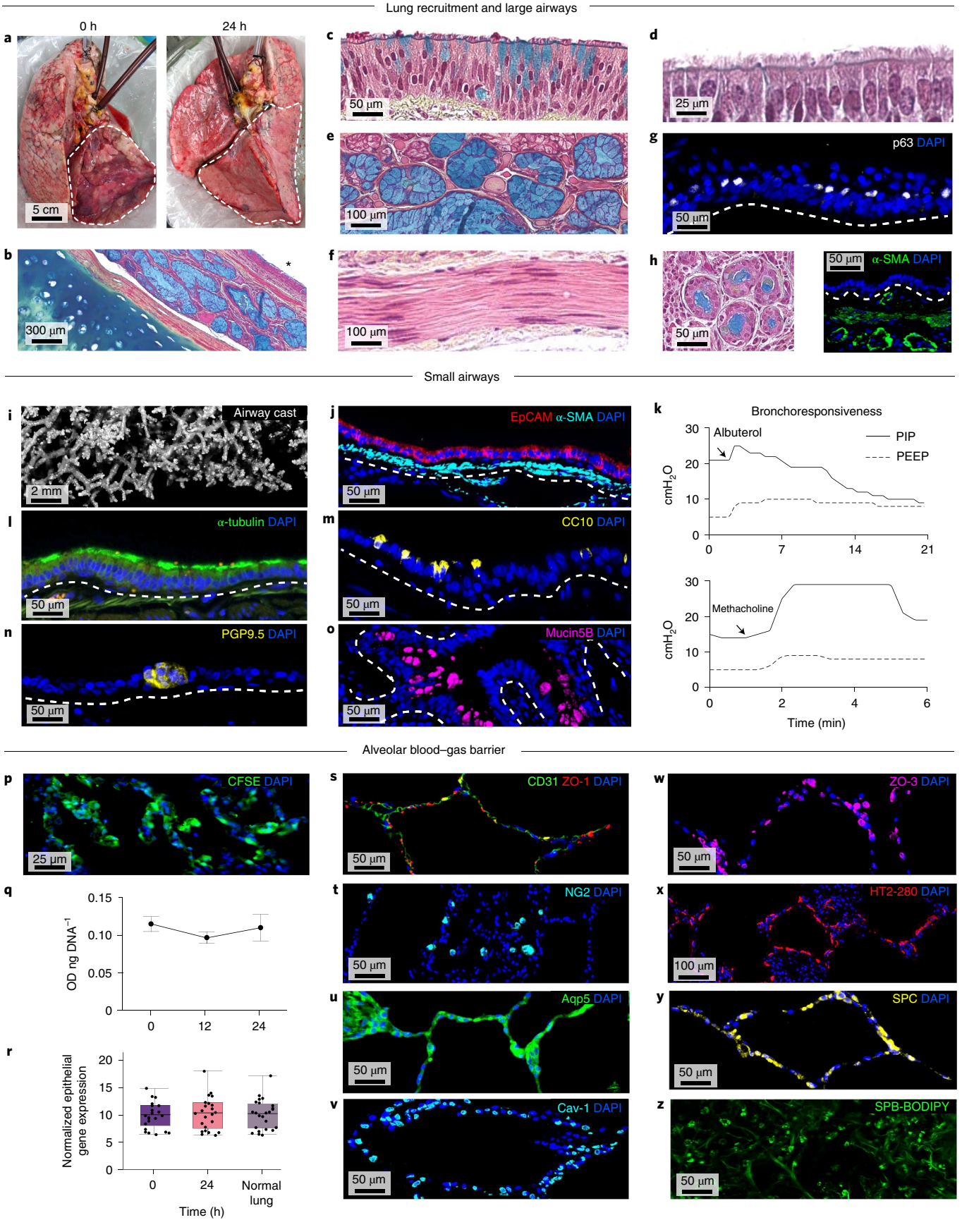

used to mitigate risk of PERV transmission[57,58]. Nevertheless, the concern for zoonotic infections cannot be discounted and further investigation is required. To assess the effects of prolonged normothermic perfusion on microbial burden, previous studies reported quantitative analyses of bacterial and fungal loads in the BAL fluid of lungs on EVLP[59]. Similar evaluations should be conducted in future preclinical studies of lungs recovered on xenogeneic cross-circulation. Overall, the clinical risks and functional and immunological outcomes that make lungs safe and acceptable for transplantation have not yet been established for xenogeneic cross-circulation. While all lungs in this study demonstrated functional and histological improvements throughout 24 h of xenogeneic cross-circulation, only lungs 3 and 4 reached $PaO_2/FiO_2 \geq 350$ mm Hg, suggesting that longer durations of cross-circulation or therapeutic intervention, may be required to improve oxygenation before transplantation. Before clinical translation, future studies should evaluate the safety, feasibility, risk profiles and outcomes of xenogeneic cross-circulation in larger series of lungs.

On the basis of the results of this study, we envision clinical applications, wherein extended criteria donor organs that cannot be recovered on EVLP could be recovered using xenogeneic cross-circulation (Extended Data Fig. 10). Critically ill patients requiring urgent lung transplantation but unable to match donor lungs may be candidates to receive lungs recovered by xenogeneic cross-circulation. For these patients, cross-circulation may represent the only opportunity to receive a life-saving lung transplantation. Alternatively, patients who await transplantation on extracorporeal membrane oxygenation support could serve as allogeneic cross-circulation 'hosts' to enable functional assessment and graft recovery of reversibly injured lungs before transplantation. Thus, cross-circulation could enable assessment and recovery of high-risk lungs without the concurrent stress of a surgical transplantation procedure. Recovered lungs would be subsequently transplanted into the host recipient.

Beyond clinical applications, the xenogeneic cross-circulation platform may also serve as a basic and translational research tool to further investigate outstanding immunological questions and enable studies of extracorporeal organ recovery, regeneration, bioengineering and advanced therapeutic interventions[6]. Modifications to the xenogeneic cross-circulation circuit could enable investigation and recovery of other human organs, including livers, hearts, kidneys and limbs. Ultimately, we envision that xenogeneic cross-circulation could be utilized as both a translational research platform to augment transplantation research and as a biomedical technology to help address the organ shortage by enabling the recovery of previously unsalvageable donor organs.

Online content

Any methods, additional references, Nature Research reporting summaries, source data, extended data, supplementary information, acknowledgements, peer review information; details of author contributions and competing interests; and statements of data and code availability are available at https://doi.org/10.1038/s41591-020-0971-8.

Received: 23 December 2019; Accepted: 9 June 2020;
Published online: 13 July 2020

References

1. World Health Organization. *World Health Statistics 2017: Monitoring Health for the SDGs, Sustainable Development Goals* (World Health Organization, 2017).
2. Chambers, D. C. et al. The international thoracic organ transplant registry of the International Society for Heart and Lung Transplantation: thirty-fifth adult lung and heart-lung transplant report—2018; focus theme: multiorgan transplantation. *J. Heart Lung Transplant.* **37**, 1169–1183 (2018).
3. Van Herck, A., Verleden, S. E., Vanaudenaerde, B. M., Verleden, G. M. & Vos, R. Prevention of chronic rejection after lung transplantation. *J. Thorac. Dis.* **9**, 5472–5488 (2017).
4. Sommer, W. et al. Extended criteria donor lungs and clinical outcome: results of an alternative allocation algorithm. *J. Heart Lung Transplant.* **32**, 1065–1072 (2013).
5. Pinezich, M. & Vunjak-Novakovic, G. Bioengineering approaches to organ preservation ex vivo. *Exp. Biol. Med.* **244**, 630–645 (2019).
6. Guenthart, B. A. et al. Cell replacement in human lung bioengineering. *J. Heart Lung Transplant.* **38**, 215–224 (2019).
7. Yamada, K. et al. Marked prolongation of porcine renal xenograft survival in baboons through the use of α-1,3-galactosyltransferase gene-knockout donors and the cotransplantation of vascularized thymic tissue. *Nat. Med.* **11**, 32–34 (2005).
8. Sykes, M. & Sachs, D. H. Transplanting organs from pigs to humans. *Sci. Immunol.* **4**, eaau6298 (2019).
9. Cypel, M. et al. Normothermic ex vivo lung perfusion in clinical lung transplantation. *N. Engl. J. Med.* **364**, 1431–1440 (2011).
10. O'Neill, J. D. et al. Cross-circulation for extracorporeal support and recovery of the lung. *Nat. Biomed. Eng.* **1**, 1–15 (2017).
11. Loor, G. et al. Prolonged EVLP using OCS lung: cellular and acellular perfusates. *Transplantation* **101**, 2303–2311 (2017).
12. Sommer, W. et al. Prediction of transplant outcome after 24-hour ex vivo lung perfusion using the organ care system in a porcine lung transplantation model. *Am. J. Transplant.* **19**, 345–355 (2019).
13. Spratt, J. R. et al. An experimental study of the recovery of injured porcine lungs with prolonged normothermic cellular ex vivo lung perfusion following donation after circulatory death. *Transpl. Int. J.* **30**, 932–944 (2017).
14. Guenthart, B. A. et al. Regeneration of severely damaged lungs using an interventional cross-circulation platform. *Nat. Commun.* **10**, 1–16 (2019).
15. Hozain, A. E. et al. Multi-day maintenance of extracorporeal lungs using cross-circulation with conscious swine. *J. Thorac. Cardiovasc. Surg.* **159**, 1640–1653 (2019).
16. Brigham, K. L. & Snell, J. D. In vivo assessment of pulmonary vascular integrity in experimental pulmonary edema. *J. Clin. Invest.* **52**, 2041–2052 (1973).
17. de Perrot, M., Liu, M., Waddell, T. K. & Keshavjee, S. Ischemia-reperfusion-induced lung injury. *Am. J. Respir. Crit. Care Med.* **167**, 490–511 (2003).
18. Slama, A. et al. Standard donor lung procurement with normothermic ex vivo lung perfusion: a prospective randomized clinical trial. *J. Heart Lung Transplant.* **36**, 744–753 (2017).
19. Warnecke, G. et al. Normothermic ex-vivo preservation with the portable organ care system lung device for bilateral lung transplantation (INSPIRE): a randomised, open-label, non-inferiority, phase 3 study. *Lancet Respir. Med.* **6**, 357–367 (2018).
20. Loor, G. et al. Portable normothermic ex-vivo lung perfusion, ventilation, and functional assessment with the organ care system on donor lung use for transplantation from extended-criteria donors (EXPAND): a single-arm, pivotal trial. *Lancet Respir. Med.* **7**, 975–984 (2019).
21. Andreasson, A. S. I. et al. Profiling inflammation and tissue injury markers in perfusate and bronchoalveolar lavage fluid during human ex vivo lung perfusion. *Eur. J. Cardio-Thorac. Surg.* **51**, 577–586 (2017).
22. Okamoto, T., Wheeler, D., Farver, C. F. & McCurry, K. R. Transplant suitability of rejected human donor lungs with prolonged cold ischemia time in low-flow acellular and high-flow cellular ex vivo lung perfusion systems. *Transplantation* **103**, 1799–1808 (2019).
23. Sadaria, M. R. et al. Cytokine expression profile in human lungs undergoing normothermic ex-vivo lung perfusion. *Ann. Thorac. Surg.* **92**, 478–484 (2011).
24. Fujino, N. et al. Isolation of alveolar epithelial type II progenitor cells from adult human lungs. *Lab. Investig. J. Tech. Methods Pathol.* **91**, 363–378 (2011).
25. Rock, J. R., Randell, S. H. & Hogan, B. L. M. Airway basal stem cells: a perspective on their roles in epithelial homeostasis and remodeling. *Dis. Model. Mech.* **3**, 545–556 (2010).
26. Tata, A. et al. Myoepithelial cells of submucosal glands can function as reserve stem cells to regenerate airways after injury. *Cell Stem Cell* **22**, 668–683 (2018).
27. Olajuyin, A. M., Zhang, X. & Ji, H.-L. Alveolar type 2 progenitor cells for lung injury repair. *Cell Death Discov.* **5**, 63 (2019).
28. Griesemer, A., Yamada, K. & Sykes, M. Xenotransplantation: immunological hurdles and progress toward tolerance. *Immunol. Rev.* **258**, 241–258 (2014).
29. Breimer, M. E. et al. Extracorporeal ('ex vivo') connection of pig kidneys to humans. I. Clinical data and studies of platelet destruction. *Xenotransplantation* **3**, 328–339 (1996).
30. Baquerizo, A. et al. Characterization of human xenoreactive antibodies in liver failure patients exposed to pig hepatocytes after bioartificial liver treatment: an ex vivo model of pig to human xenotransplantation 1,2. *Transplantation* **67**, 5 (1999).

31. Levy, M. F. et al. Liver allotransplantation after extracorporeal hepatic support with transgenic (hCD55/hCD59) porcine livers: clinical results and lack of pig-to-human transmission of the porcine endogenous retrovirus 1. *Transplantation* **69**, 272 (2000).
32. Li, Q. et al. Is sensitization to pig antigens detrimental to subsequent allotransplantation? *Xenotransplantation* **25**, e12393 (2018).
33. Scheffert, J. L. & Raza, K. Immunosuppression in lung transplantation. *J. Thorac. Dis.* **6**, 1039–1053 (2014).
34. Cochrane, C. G., Müller-Eberhard, H. J. & Aikin, B. S. Depletion of plasma complement in vivo by a protein of cobra venom: its effect on various immunologic reactions. *J. Immunol.* **105**, 55–69 (1970).
35. OBERHOLZER, J. et al. Decomplementation with cobra venom factor prolongs survival of xenografted islets in a rat to mouse model. *Immunology* **97**, 173–180 (1999).
36. Haihua, C., Wei, W., Kun, H., Yuanli, L. & Fei, L. Cobra venom factor-induced complement depletion protects against lung ischemia reperfusion injury through alleviating blood-air barrier damage. *Sci. Rep.* **8**, 1–8 (2018).
37. Gorsuch, W. B., Guikema, B. J., Fritzinger, D. C., Vogel, C.-W. & Stahl, G. L. Humanized cobra venom factor decreases myocardial ischemia reperfusion injury. *Mol. Immunol.* **47**, 506–510 (2009).
38. Campos, M. M. et al. The role of migrating leukocytes in IL-1β-induced up-regulation of kinin B1 receptors in rats. *Br. J. Pharmacol.* **135**, 1107–1114 (2002).
39. Bickel, M. The role of interleukin-8 in inflammation and mechanisms of regulation. *J. Periodontol.* **64**, 456–460 (1993).
40. De Perrot, M. et al. Interleukin-8 release during early reperfusion predicts graft function in human lung transplantation. *Am. J. Respir. Crit. Care Med.* **165**, 211–215 (2002).
41. Andreasson, A. S. I. et al. The role of interleukin-1β as a predictive biomarker and potential therapeutic target during clinical ex vivo lung perfusion. *J. Heart Lung Transplant.* **36**, 985–995 (2017).
42. Scheller, J., Chalaris, A., Schmidt-Arras, D. & Rose-John, S. The pro- and anti-inflammatory properties of the cytokine interleukin-6. *Biochim. Biophys. Acta Mol. Cell Res.* **1813**, 878–888 (2011).
43. Halloran, P. F. et al. IFN-γ alters the pathology of graft rejection: protection from early necrosis. *J. Immunol.* **166**, 7072–7081 (2001).
44. Kawut, S. M. et al. Soluble P-selectin and the risk of primary graft dysfunction after lung transplantation. *Chest* **136**, 237–244 (2009).
45. Loss, M. et al. Acute vascular rejection is associated with systemic complement activation in a pig-to-primate kidney xenograft model. *Xenotransplantation* **7**, 186–196 (2000).
46. McCurry, K. R. et al. Humoral responses to pig-to-baboon cardiac transplantation: implications for the pathogenesis and treatment of acute vascular rejection and for accommodation. *Hum. Immunol.* **58**, 91–105 (1997).
47. Zuber, J. & Sykes, M. Mechanisms of mixed chimerism-based transplant tolerance. *Trends Immunol.* **38**, 829–843 (2017).
48. Kuwaki, K. et al. Heart transplantation in baboons using α-1,3-galactosyltransferase gene-knockout pigs as donors: initial experience. *Nat. Med.* **11**, 29–31 (2005).
49. Lee, K. et al. Engraftment of human iPS cells and allogeneic porcine cells into pigs with inactivated RAG2 and accompanying severe combined immunodeficiency. *Proc. Natl Acad. Sci. USA* **111**, 7260–7265 (2014).
50. Pan, H. et al. Lymphodepletive effects of rabbit anti-pig thymocyte globulin in neonatal swines. *Transpl. Immunol.* **39**, 74–83 (2016).
51. Bottino, R. et al. Safe use of anti-Cd154 monoclonal antibody in pig islet xenotransplantation in monkeys. *Xenotransplantation* **24**, e12283 (2017).
52. Nottle, M. B. et al. Targeted insertion of an anti-CD2 monoclonal antibody transgene into the *GGTA1* locus in pigs using *Fok* I-dCas9. *Sci. Rep.* **7**, 1–8 (2017).
53. Boneva, R. S. & Folks, T. M. Xenotransplantation and risks of zoonotic infections. *Ann. Med.* **36**, 504–517 (2004).
54. Noordergraaf, J. et al. Pathogen elimination and prevention within a regulated, designated pathogen free, closed pig herd for long-term breeding and production of xenotransplantation materials. *Xenotransplantation* **25**, e12428 (2018).
55. Denner, J. The porcine virome and xenotransplantation. *Virol. J.* **14**, 171 (2017).
56. Godehardt, A. W., Costa, M. R. & Tönjes, R. R. Review on porcine endogenous retrovirus detection assays—impact on quality and safety of xenotransplants. *Xenotransplantation* **22**, 95–101 (2015).
57. Niu, D. et al. Inactivation of porcine endogenous retrovirus in pigs using CRISPR-Cas9. *Science* **357**, 1303–1307 (2017).
58. Dieckhoff, B. et al. Knockdown of porcine endogenous retrovirus (PERV) expression by PERV-specific shRNA in transgenic pigs. *Xenotransplantation* **15**, 36–45 (2008).
59. Andreasson, A. et al. The effect of ex vivo lung perfusion on microbial load in human donor lungs. *J. Heart Lung Transplant.* **33**, 910–916 (2014).

Methods

Study design. The study was designed as a proof-of-feasibility study ($n=6$) to assess the ability of the xenogeneic cross-circulation system to maintain and recover the quality and function of explanted human lungs for 24 h. As explanted human lungs are susceptible to injury, dysregulation and loss of respiratory function without adequate support, 24 h was deemed a sufficient duration of extracorporeal support to assess the feasibility of xenogeneic cross-circulation. Our hypothesis was that xenogeneic cross-circulation between explanted human lungs and a swine host could provide a systemic environment that supports lung maintenance and recovery for 24 h. The study included two experimental groups: (1) with immunosuppression ($n=5$) and (2) without immunosuppression ($n=1$ as an immunological control) and was conducted with the minimum number of animals to demonstrate feasibility and reproducibility between lungs and across experimental time points. Data from the study can be used to conduct power analyses for subsequent investigations. All samples were collected and analyzed in triplicate.

Animals. Yorkshire swine ($n=6$) were 5–8 months of age, with a mean weight of 62.3 ± 1.4 kg (range, 61.4–64.0 kg). As experimental xenogeneic cross-circulation procedures were conducted at sites in Columbia University and Vanderbilt University, the study received approvals from the Institutional Animal Care and Use Committee at both Columbia University and Vanderbilt University. All animal care and procedures were conducted in accordance with the US National Research Council of the National Academies Guide for the Care and Use of Laboratory Animals, Eighth Edition.

Immunosuppression. To assess the feasibility of conducting xenogeneic cross-circulation without immunosuppression, immunosuppressive drugs were not administered before or during xenogeneic cross-circulation ($n=1$). Lack of immunosuppression resulted in severe acute rejection in less than 1 h and practically prohibited xenogeneic cross-circulation. Consequently, to reduce risk of immunological rejection and enable xenogeneic cross-circulation, an immunosuppression regimen informed by established protocols[14,15] and current practices in clinical lung transplantation[33] was implemented, and immunosuppression drugs were administered before and during xenogeneic cross-circulation ($n=5$). Induction immunosuppression consisted of a conventional combination of calcineurin inhibitor (tacrolimus) and antiproliferative agent (mycophenolate). Mycophenolate (500 mg; Roche) and tacrolimus (0.4 mg kg^{-1}; Sandoz) were administered per os twice a day for at least 14 d before initiation of xenogeneic cross-circulation. Enrofloxacin (5 mg kg^{-1}; Henry Schein) and cephalexin (25 mg kg^{-1}; Zoetis) were also administered to reduce risk of infection during induction of immunosuppression. At 4 h before initiation of xenogeneic cross-circulation, swine hosts were sedated, intubated and administered intravenous diphenhydramine (50 mg; Henry Schein), methylprednisolone (1 g; Henry Schein) and administered CVF (1 mg; Sigma-Aldrich) to deplete complement activity[34,36]. Both diphenhydramine and methylprednisolone were given to limit anaphylactic response associated with CVF administration. Immediately before the start of xenogeneic cross-circulation, tacrolimus (5 mg; Sandoz), methylprednisolone (125 mg; Henry Schein) and mycophenolate (500 mg; Roche) were administered intravenously to inhibit innate and adaptive immune responses. Methylprednisolone was subsequently re-administered at 8 h and 16 h. Tacrolimus and mycophenolate were re-administered at 12 h (Extended Data Fig. 1b). Blood samples were collected every 1–4 h to assess circulating levels of immunosuppression drugs. Complement activity was quantified by CH50 assay (EZ Complement CH50 Test; Diamedix). Tacrolimus (FK506) levels were quantified (Architect System; Abbott) to ensure maintenance of therapeutic levels throughout xenogeneic cross-circulation.

Human lung donors. Donor lungs ($n=6$) unacceptable for clinical transplantation and consented for use in research were procured in coordination with local organ procurement organizations under protocols approved by the Institutional Review Board at Columbia University Medical Center and Vanderbilt University Medical Center. Deidentified donor data were obtained through the United Network for Organ Sharing under the approved protocols. Donors were excluded on the basis of the following criteria: severe purulent secretions on bronchoscopy; history of infection with human immunodeficiency virus, hepatitis B/C and methicillin-resistant *Staphylococcus aureus*.

Procurement of human lungs. When human lungs acceptable for the study were identified, a team was dispatched from Columbia University Medical Center or Vanderbilt University Medical Center to procure lungs in standard fashion. All lung procurements were performed in coordination with other teams dedicated to procurement of organs (for example, heart, kidney and liver) for clinical transplantation. At the time of procurement, a bolus of heparin (30,000 U) was administered intravenously, the aorta was clamped and cold low-potassium dextran solution (Perfadex; Vitrolife) with alprostadil (25 mg kg^{-1}, Prostin VR Pediatric; Pfizer) was administered through the pulmonary artery as an anterograde flush. The chest was packed with sterile ice slush to achieve topical cooling, lungs were inflated to an airway pressure of 15 cmH_2O, and the trachea was stapled (DST TA; Medtronic). Lungs were then explanted and placed in a sterile isolation bag with 500 ml of organ preservation solution (Perfadex; Vitrolife) at 4 °C. The bag was placed in a second sterile isolation bag containing 1 l of normal saline at 4 °C and subsequently placed on ice.

Cannulation of explanted human lungs. After explant, lungs were transported on ice to the research operating room at Columbia University Medical Center or Vanderbilt University Medical Center and placed on the back table on ice for preparation. Notably, because the heart was procured for clinical transplantation from three donors (donors 1, 3 and 6) and the contralateral lung was procured for clinical transplantation from two donors (donors 4 and 5), segments of the structures connecting the heart and lungs (left atrial cuff and main pulmonary artery), were procured for transplantation, resulting in minimal (1–3 mm) circumferential left atrial cuff and truncated or no main pulmonary artery. Consequently, reconstruction of the left atrial cuff and/or pulmonary artery was required in some cases (Supplementary Fig. 5). Donor pericardium, descending thoracic aorta or polyethylene terephthalate grafts (Dacron; Maquet) were used to facilitate cannulation of explanted human lungs at the pulmonary artery and left atrial cuff. After reconstruction, the pulmonary artery and left atrial cuff were cannulated as previously described[10,14,15] and cold sterile isotonic electrolyte-balanced solution was flushed through the lungs to prime arterial and venous cannulas. A basin lined with two sterile isolation bags and filled with warm saline was placed in the organ preservation chamber, which was equipped with a heater and humidifier to maintain normothermic physiologic conditions similar to those in the thoracic cavity. A top-loading balance (Denver Instrument Company) was inserted beneath the basin to enable lung weight measurements. After cannulation, lungs were placed in the basin in prone position and cannulas were secured.

Xenogeneic cross-circulation between explanted human lungs and swine host. All swine hosts ($n=6$) underwent general anesthesia by intramuscular induction with tiletamine/zolazepam (5 mg kg^{-1}, Telazol; Zoetis). Anesthesia was maintained with continuous intravenous infusions of fentanyl citrate (0.1 mg kg^{-1} h^{-1}; West Ward Pharmaceuticals), midazolam (1.5 mg kg^{-1} h^{-1}; Akorn) and inhaled isoflurane (1–5% in oxygen; Henry Schein). Cefazolin (30 mg kg^{-1}; Sandoz) and enrofloxacin (5 mg kg^{-1}; Henry Schein) were administered before skin incision and re-administered every 8 h and 24 h, respectively. An auricular or femoral arterial line (Arrow International) was placed for hemodynamic monitoring and periodic blood sampling. Bilateral neck cut-downs exposed the left and right internal jugular veins. A heparin bolus (30,000 U) was administered, and cannulas (18 French; Medtronic) were placed in the internal jugular veins using the Seldinger technique. Calcium chloride (1 g; Henry Schein) was then administered, and explanted human lungs were connected to the circuit via cannulas secured in the pulmonary artery and vein, thereby marking the start of xenogeneic cross-circulation. Initial flow rates were maintained within 5–10% of estimated cardiac output of the swine host, with target pulmonary artery pressure <15 mm Hg and pulmonary vein pressure 3–5 mm Hg. Pressure at the pulmonary veins was dependent on the hydrostatic pressure difference between the lungs and swine host and was controlled by adjusting the height difference between the lungs and swine host (target, 10 cm). As swine hosts were anesthetized and therefore immobile for the duration of all procedures, the height difference that yielded target pressure values was set at the beginning of each procedure and rarely required adjustment. Controlled adjustments of lung height were performed as needed using a hydraulic lift. Perfusion circuit elements consisted of a main console (Jostra HL-20 pump console; Maquet), disposable pump (Rotaflow centrifugal pump; Maquet), softshell reservoir (Maquet) and sterile pre-packaged single-use disposable three-eighths inch flexible tubing (smart coated tubing; LivaNova). All single-use disposable circuit components were replaced before each procedure. Pressures (PA and PV), flows (PA and PV) and perfusate temperatures were continuously monitored and recorded (VIPER clinical interfacing software G2 v.1.26.4; Spectrum Medical). Throughout the duration of xenogeneic cross-circulation, swine hosts were maintained with a continuous heparin infusion (initial rate: 25 U kg^{-1} h^{-1}). Activated clotting time was measured using a whole-blood microcoagulation system (Hemochron; Accriva Diagnostics), and the heparin drip was adjusted to maintain activated clotting times within the target range of 250–350 s. Physiological parameters of the swine host, including heart rate, electrocardiogram, blood pressure (cuff and arterial line pressure), mean arterial pressure, oxygen saturation (SpO_2), end-tidal CO_2, temperature and respiratory rate, were continuously monitored and recorded (Supplementary Table 1) using a multiparameter vital signs monitor (SurgiVet).

Ventilation of explanted human lungs. *Ventilation strategy.* The circuit and lungs were allowed to acclimate to normothermic temperature, and ventilation was initiated within the first 10 min of cross-circulation, with the following initial settings: volume control mode; respiratory rate, 6–8 breaths min^{-1}; tidal volume, 6 ml kg^{-1}; PEEP, 5 cmH_2O; and FiO_2, 40% (Oxylog 3000 plus; Dräger). Continuous time-lapse photography (1 frame min^{-1}) was captured with a high-resolution camera (Hero4 Black 4 K; GoPro, Supplementary Video 1).

Alveolar recruitment. Atelectatic lung regions were recruited by gradually increasing tidal volume by 15–20%, increasing PEEP up to 10 cmH_2O and performing inspiratory holds (sustained inflation) with peak inspiratory pressures up to 25 cmH_2O. If ventilator adjustments were insufficient to recruit lung regions, manual recruitment maneuvers were performed by an experienced lung transplant surgeon in a manner consistent with standard practices used during clinical lung transplantation. During inspiration, gentle manual compression was applied to areas of aerating lung, thereby directing ventilation toward areas of nonaerating atelectatic lung to transiently increase the local airway pressure gradient, resulting in recruitment of nonaerated lung volume and increased vital capacity, while avoiding barotrauma and the deleterious effects of hyperinflation. Alveolar recruitment was performed as needed, and lungs underwent a maximum recruitment time of approximately 30 min, during which peak inspiratory pressures were monitored and maintained <30 cmH_2O.

Functional analyses of explanted human lungs. Blood samples were collected from the main pulmonary artery cannula (blood entering left and right lungs), main PV cannula (blood exiting left and right lungs) every 6 h, and hemogas analysis was performed using a point-of-care blood analysis system (epoc; Siemens Healthineers). Dynamic compliance (C_{dyn} = TV/(PIP − PEEP)) and PaO_2/FiO_2 were calculated every 6 h. Lung weight was obtained every 6 h using a top-loading balance (Denver Instrument Company) inside the organ chamber. The organ basin and contents were tared at each time point to ensure accurate measurements. Radiographs of explanted human lungs were acquired using a portable X-ray unit (PXP-16HF; United Radiology Systems) at 2.2 mAs and 90 kVp.

Histopathological analysis. *Tissue sample collection.* Before the start of each experiment, a lung map with predetermined regions (eight regions per left or right lung) was generated, and each region was assigned an arbitrary number, as previously described[10]. Accordingly, to avoid sampling bias, the location of lung wedge tissue sample collections was randomized using a random number generator (www.random.org). A surgical stapler (GIA Auto Suture; Covidien) with medium/thick reloads was used to obtain lung samples at 0, 12 and 24 h of xenogeneic cross-circulation. Specimens were immediately fixed in cold 4% paraformaldehyde for 48–72 h, embedded in paraffin and sectioned at 3-μm or 5-μm thickness. Comparative specimens of deidentified human lung tissue trimmed at the time of transplantation were obtained as paraffin-embedded blocks from the Department of Anatomical Pathology under a protocol approved by the Institutional Review Board at Columbia University Medical Center. All sections were stained with H&E and examined under light microscopy. Additional sections were stained with silver reticulin, Alcian blue (pH 2) and pentachrome by the histology service in the Department of Molecular Pathology at Columbia University Medical Center.

Blinded pathologic review. Pathologic review was performed by an experienced lung transplant pathologist blinded to the study protocol. All slides (H&E, immunohistochemical staining for neutrophil elastase, caspase 3 and TUNEL) were randomized, arbitrarily numbered and delivered to the pathologist without reference to experimental time points or conditions. An established lung injury scoring rubric[10,14,15] was used to score each sample (Supplementary Table 2). Scoring criteria were based on histologic analyses of hpf (×40, 0.2 $mm)^2$.

Airway polymorphonuclear cells were evaluated as bronchi and bronchioles containing any neutrophils per hpf (0 ⇒ 0%; 1 ⇒ 1–25%; 2 ⇒ 26–50%; 3 ⇒ >50%). Alveolar polymorphonuclear cells were evaluated as alveoli more than half-filled with neutrophils per hpf (0 ⇒ 0%; 1 ⇒ 1–25%; 2 ⇒ 26–50%; 3 ⇒ >50%). Alveolar edema was evaluated as alveoli with edema per hpf (0 ⇒ <5%; 1 ⇒ 6–25%; 2 ⇒ 26–50%; 3 ⇒ >50%). Interstitial infiltrate was evaluated as the number of lymphocytes and neutrophils in the interstitium around vessels and airways and in alveolar septa and pleura per hpf (0 ⇒ 0; 1 ⇒ <50; 2 ⇒ 50–100; 3 ⇒ >100). Interstitial edema was evaluated as expansion of perivascular and peribronchial spaces with edematous fluid, relative to the width of vessel medium, per hpf (0 ⇒ none; 1 ⇒ 1× width vessel medium; 2 ⇒ ≥2× width vessel medium). Apoptotic cells were evaluated as the percent of early (caspase 3^+) and late ($TUNEL^+$) apoptotic cells relative to the total number of cells per hpf (0 ⇒ 0–5; 1 ⇒ 6–10; 2 ⇒ 11–15; 3 ⇒ >15).

Immunohistochemical staining. Human lung sections were de-paraffinized, incubated in boiling citrate buffer (pH 6.0) for antigen retrieval for 15 min and blocked with 10% normal goat serum in phosphate-buffered saline for 2 h at room temperature. Primary antibodies were added and incubated for 12 h at 4 °C or 4 h at 25 °C. For all immunostains, the secondary antibody was diluted 1:200 and incubated for 1 h at 25 °C. Sections were mounted in mounting medium (Vectashield Mounting Medium; Vector Laboratories) with DAPI, coverslipped and imaged with a fluorescence microscope (DMi8; Leica). Immunostaining was performed by Molecular Pathology Histology Services in the Herbert Irving Comprehensive Cancer Center at Columbia University Medical Center. A list of antibodies and dilutions used is in Supplementary Table 13.

Electron microscopy. *Scanning electron microscopy.* Lung tissue samples were obtained at 0, 12 and 24 h of xenogeneic cross-circulation, fixed in formalin, rinsed in 70% ethanol, frozen and lyophilized. Samples were imaged using a scanning electron microscope (GeminiSEM 300; Zeiss) with accelerating voltage of 2.5 kV.

Transmission electron microscopy. Lung tissue samples were obtained at 0, 12 and 24 h of xenogeneic cross-circulation, fixed with 2.5% glutaraldehyde, 4% paraformaldehyde and 0.02% picric acid in 0.1 M sodium cacodylate buffer (pH 7.2). Samples were then post-fixed with 1% OsO_4 in Sorenson's buffer for 1 h, dehydrated and embedded in Lx-112 (Ladd Research Industries). Sections (thickness of 60 nm) were prepared using an ultramicrotome (PowerTome PT XL; RMC), stained with uranyl acetate and lead citrate and examined with a transmission electron microscope (JEM-1200 EXII; JEOL). Images were captured with a digital camera (ORCA-HR; Hamamatsu) and recorded with imaging software (Image Capture Engine v.602.569; AMT).

BAL fluid analyses. *BAL fluid sample collection.* BAL fluid samples were collected every 6 h by wedging a 3.8-mm flexible video bronchoscope (aScope 3; Ambu) into a subsegmental bronchus of the left and right lower lobes of each set of lungs. Sterile normal saline (5 ml) was injected, aspirated and collected in a sterile specimen trap (Busse Hospital Disposables). Gross photographs of BAL fluid samples were acquired using a digital camera (Sony). The pH of BAL fluid samples was measured with a glass double-junction microelectrode (Thermo Fisher Scientific). BAL fluid samples were then centrifuged at 3,500 r.p.m. for 10 min at 4 °C. Supernatants were collected and stored at −80 °C until further processing. Cultures from BAL fluid samples were analyzed for bacterial and fungal growth at baseline and 24 h (Antech Diagnostics).

Cytopathology. Cellular contents of BAL fluid samples were visualized by periodic acid-Schiff staining of BAL fluid smears.

Molecular pathology. Total protein concentrations in BAL fluid were quantified by protein assay (Pierce Coomassie Bradford Protein Assay Kit; Thermo Fisher Scientific) according to the manufacturer's instructions. Inflammatory markers in BAL fluid collected from explanted left and right human lungs (Supplementary Tables 3–7) were analyzed in triplicate by multiplex cytokine array (Human Cytokine/Chemokine 65-Plex Panel; Eve Technologies).

Immunologic analyses. *Blood analyses.* Blood samples were collected every 6 h from an auricular arterial line (or femoral arterial line if auricular placement was unsuccessful). Blood gas analysis was performed using a point-of-care blood analysis system (epoc; Siemens Healthineers). Blood samples were collected in blood collection tubes (BD Vacutainer) and analyzed by a diagnostic laboratory (Antech Diagnostics) for complete blood count, comprehensive metabolic panel and coagulation panel (Supplementary Table 1). Serum inflammatory markers (granulocyte–macrophage colony-stimulating factor, IFN-γ, IL-1α, IL-1β, IL-1ra, IL-2, IL-4, IL-6, IL-8, IL-10, IL-12, IL-18 and TNF-α) were analyzed in triplicate by multiplex cytokine array (Discovery Assay Pig Cytokine Array; Eve Technologies; Supplementary Table 9). Hemolytic markers (D-dimer, fibrinogen and plasma-free hemoglobin) and P-selectin were analyzed in triplicate by ELISA. A list of ELISA kits used is in Supplementary Table 14.

Lung tissue analyses. Tissue samples were collected from left and right human lungs at 0, 12 and 24 h of xenogeneic cross-circulation with and without immunosuppression. For quantitative cellular analyses, tissue samples were immunostained for α-Gal (LS-C63415; LS Bio), CD45 (ab0559; Abcam), CD163 (ab87099; Abcam), HNA (ab190710; Abcam) and neutrophil elastase (ab68672; Abcam). Slides were randomized, arbitrarily numbered and delivered without reference to experimental time points or conditions to a reviewer blinded to the study protocol. Quantification of cells was based on cell counts per hpf (×40, 0.2 mm^2)

Functional tests and assays. *Bronchoresponsiveness test.* The effects of methacholine and albuterol on airway smooth muscle tone were assessed after 24 h of xenogeneic cross-circulation. To ensure that responses were definitively from explanted human lungs, all bronchoresponsiveness tests were conducted shortly after human lungs were disconnected from cross-circulation with swine host and maintained on isolated EVLP. Methacholine (100 mg kg^{-1}; Methapharm) and albuterol (3 mg; Nephron) were administered to explanted human lungs by nebulizer. Airway pressures were continuously recorded to assess changes in peak inspiratory pressures in response to cholinergic or β1/2 agonistic effects of methacholine or albuterol, respectively.

Vasoresponsiveness test. The effect of selective α_1-adrenergic receptor activation resulting in vasoconstriction of pulmonary vasculature was assessed after 24 h of xenogeneic cross-circulation. To ensure that responses were definitively from explanted human lungs, vasoresponsiveness tests were conducted shortly after human lungs were disconnected from cross-circulation with swine host and maintained on isolated EVLP. Phenylephrine (4 mg; International Medication Systems) was administered intravenously into the pulmonary artery cannula of explanted human lungs, and vascular pressures and flows were continuously recorded to assess the changes in pulmonary artery and vein pressures.

CFSE uptake assay. To assess viability of the pulmonary endothelium in explanted human lungs, CFSE (Affymetrix) was reconstituted in dimethyl sulfoxide at a concentration of 1.06 M, protected from light and delivered via intravascular injection with a 20-Ga needle after 24 h of xenogeneic cross-circulation. After 15 min of incubation, lung tissue samples were washed five times with phosphate-buffered saline, fixed in cold phosphate-buffered 4% paraformaldehyde for 48 h, embedded, de-paraffinized and imaged as previously described.

Acetylated low-density lipoprotein uptake assay. To assess function of the pulmonary endothelium in explanted human lungs, biopsies (4 mm) of the left and right pulmonary arteries and pulmonary veins were collected and placed in a 96-well plate (BD Falcon). Then, aLDL with fluorescent Alexa Fluor 594 conjugate (L35353; Thermo Fisher Scientific) was diluted 1:200 in 1× DMEM/F12K cell culture medium (Corning). Wells containing pulmonary vascular tissue biopsies from each lung received 150 µl of medium with aLDL reagent or medium alone (negative control). The multiwell plate was covered with aluminum foil and incubated at 37 °C with gentle shaking for 4 h. After incubation, samples were washed five times with phosphate-buffered saline, fixed in cold phosphate-buffered 4% paraformaldehyde for 48 h, embedded in paraffin, sectioned at 5-µm thickness, de-paraffinized, stained with DAPI and imaged using a fluorescence microscope (FSX100; Olympus).

Surfactant-BODIPY uptake assay. To assess viability and functional uptake of type II pneumocytes, fluorescent SPB-BODIPY was delivered into distal regions of explanted human lungs after 24 h of xenogeneic cross-circulation using a flexible bronchoscope and microcatheter system (Renegade; Boston Scientific). After incubation for 30 min, a surgical stapler with medium/thick reloads (Medtronic) was used to collect lung tissue samples. Samples were dissected, rinsed in Dulbecco's phosphate-buffered saline and imaged immediately with a fluorescence microscope (FSX100; Olympus). Additional images were obtained by incubating end-point lung tissue samples (2 mm^3) with SPB-BODIPY (20 ng ml^{-1}) for 30 min at room temperature. Specimens were then stained with plasma-membrane stain (CellMask Deep Red; Thermo Fisher Scientific) for 10 min, followed by five washes with Dulbecco's phosphate-buffered saline. Images were acquired with a two-photon confocal laser scanning microscope (TCS SP8; Leica). Visualization of fluorescence signal in punctate patterns indicated surfactant uptake and storage in lamellar bodies of type II pneumocytes.

Metabolic activity assay. To assess changes in metabolic activity of explanted human lungs, parenchymal lung tissue samples were collected at 0, 12 and 24 h of xenogeneic cross-circulation. Tissue samples (~250 µl; $n=3$ per lung) were dissected in a sterile fashion, finely minced, gently homogenized and placed in a 96-well plate. Cell viability reagent (AlamarBlue Assay; Thermo Fisher Scientific) was diluted 1:10 in DMEM with 10% FBS. Wells containing lung sample homogenates from each lung received 100 µl of AlamarBlue reagent. Wells containing no lung homogenate (negative control) also received 100 µl of AlamarBlue reagent. The multiwell plate was covered with aluminum foil and incubated at 37 °C with gentle shaking for 2 h. After incubation, well supernatants were transferred into new 96-well plates, and absorbance was measured at 570 nm and normalized to 600 nm. To normalize metabolic activity for comparison across samples and time points, the DNA content of each sample was quantified using a DNA quantification assay (Quanti-iT PicoGreen dsDNA Assay; Invitrogen) according to the manufacturer's instructions. Samples were digested in papain (250 µg ml^{-1}) at 60 °C for 4 h and mixed with PicoGreen reagent. Fluorescence emission was measured at 520 nm with excitation at 480 nm, and DNA was quantified using a standard curve.

Airway casts. After 24 h of xenogeneic cross-circulation, explanted human lungs were disconnected from the cross-circulation system, and the airway compartment was cast with polyurethane (Underwriters Laboratories). Casting material was prepared as a foam mixture of polyurethane and acetone (4:1) with 1 ml of organic dye (Polytek Development Corp) and introduced through the endotracheal tube into explanted human lungs using a syringe. Casts were cured overnight at 4 °C. Lungs with airway casts were subsequently submerged in 30% sulfuric acid solvent for 15 d to remove surrounding lung tissues from the cast. Sulfuric acid solvent was replaced every 5 d. After 15 d, airway casts were rinsed with water, allowed to dry at 25 °C and imaged with a digital camera (Sony).

RNA sequencing. Explanted human lung tissue samples (~100 mg, $n=3$ per time point) were collected, snap-frozen in liquid nitrogen and stored at −80 °C. Samples were shipped on dry ice to an RNA sequencing service provider (Genewiz) for RNA extraction and library preparation with polyA selection. RNA samples were sequenced with a 2×150 bp configuration and single index per lane (HiSeq; Illumina). Low-quality reads and sequencing artifacts were eliminated. Sequencing reads were trimmed (Trimmomatic v.0.36; Usadel Lab)[60] to remove possible adaptor sequences and nucleotides of poor quality, then aligned to human reference genome GRCh38/hg38 (STAR aligner v.2.5.2b)[61]. Raw read counts were normalized by variance stabilizing transformation (DESeq2)[62], and differential gene expression was analyzed. Heat maps with Euclidian-based distance were generated to visualize gene expression (Pheatmap v.1.08 in R v.3.6.0), and a volcano plot was generated to visualize differentially expressed genes (EnhancedVolcano package in R v.3.6.0; Bioconductor)[63]. Gene ontology analysis was performed to assess changes in gene clusters (GeneSCF v.1.1-p2)[64]. To enable transcriptomic comparison of explanted human lungs subjected to 24 h of xenogeneic cross-circulation with normal human lungs, RNA sequencing of tissue samples from representative normal human lungs ($n=50$, randomly selected) was accessed through the Genotype-Tissue Expression project[65] via the dbGaP Portal using the dbGaP accession code phs000424.v7.p2.

Randomization of sampling. To avoid sampling bias, the location of lung wedge tissue sample collections was randomized using a random number generator (www.random.org). Before the start of each experiment, a lung map with predetermined regions (eight regions per left or right lung) was generated and each region was assigned an arbitrary number, as previously described[10]. Throughout all procedures, samples were collected at each time point according to the lung map regions that corresponded to the randomly generated numbers.

Blinded review. All analytical assessments were blinded to the maximum practical extent. All pathologic analyses were performed by an independent expert to eliminate bias.

Statistics and reproducibility. No data were excluded from analysis. One-way analysis of variance and Student's *t*-tests were performed using statistical analysis software (Prism 8.2.1; GraphPad) and $P<0.05$ was considered statistically significant. The Reporting Summary contains additional information about the experimental design and analysis. Additional details about experimental reproducibility are described below. Figure 2: results were reproduced for all lungs ($n=5$ independent experiments). Figure 3a–e: results and images were reproduced for all lungs ($n=5$ independent experiments) and are shown in Extended Data Figs. 2–9. Figure 3f,g: results and images were reproduced for lungs 1–3 ($n=3$ independent experiments) and are shown in Extended Data Figs. 7–9. Figure 3j: results and images were produced from lung 1 ($n=1$). Figure 4a,b: results and images were reproduced for two independent experiments. Figure 4c: results and images were reproduced for all lungs ($n=5$ independent experiments). Figure 4d,e,h,i,k,p: results and images were reproduced for three independent experiments. Figure 4j: the result and image was produced from one independent experiment. Figure 5a: images were reproduced for all lungs ($n=5$ independent experiments). Figure 5b–d,h: results and images were reproduced for two independent experiments. Figure 5g,h,j,l–p,s–z: results and images were reproduced for lungs 1–3 ($n=3$ independent experiments).

Reporting Summary. Further information on research design is available in the Nature Research Reporting Summary linked to this article.

Data availability

The authors declare that all data supporting the findings of this study are available within the text, figures and Supplementary Information.

References

60. Bolger, A. M., Lohse, M. & Usadel, B. Trimmomatic: a flexible trimmer for Illumina sequence data. *Bioinforma. Oxf. Engl.* **30**, 2114–2120 (2014).
61. Dobin, A. et al. STAR: ultrafast universal RNA-seq aligner. *Bioinforma. Oxf. Engl.* **29**, 15–21 (2013).
62. Love, M. I., Huber, W. & Anders, S. Moderated estimation of fold change and dispersion for RNA-seq data with DESeq2. *Genome Biol.* **15**, 550 (2014).
63. Blighe, K., Rana, S. & Lewis, M. *EnhancedVolcano: Publication-ready Volcano Plots with Enhanced Colouring and Labeling*. Bioconductor version: release (3.10) https://doi.org/10.18129/B9.bioc.EnhancedVolcano (2019).
64. Subhash, S. & Kanduri, C. GeneSCF: a real-time based functional enrichment tool with support for multiple organisms. *BMC Bioinf.* **17**, 365 (2016).
65. GTEx Consortium. The genotype-tissue expression (GTEx) project. *Nat. Genet.* **45**, 580–585 (2013).

Acknowledgements

The authors thank the following collaborators and supporters: Institute of Comparative Medicine veterinary staff, including A. Hubbard, S. Robertson, R. Ober, A. McLuckie, N. Herndon, D. Ordanes and A. Rivas for supporting animal studies; Weill Cornell Microscopy and Image Analysis Core Facility staff, including L. Cohen-Gould and J. P. Jimenez for transmission electron microscopy imaging services; Rockefeller University Electron Microscopy Resource Center staff, including K. Uyru and N. Soplop for scanning electron microscopy imaging services; Herbert Irving Comprehensive Cancer Center Molecular Pathology Shared Resources, including T. Wu, D. Sun and R. Chen for histology services; S. Chicotka, P. Liou, M. Foley, J. Diaz, M.S. Fultz, J. Adcock, N. Llore, E. Lopes, G. Pierre and I. Fedoriv for technical and analytical support; S. Pistilli, K.

Fragoso and S. Halligan for administrative support. The authors gratefully acknowledge funding support from the National Institutes of Health (EB27062, HL007854, HL120046, HL134760), Mikati Foundation and Blavatnik Foundation (STAR grant).

Author contributions

A.E.H., J.D.O., R.D., A.D.G., B.A.G., G.V.-N. and M.B. designed the study. A.E.H., J.D.O., M.R.P., Y.T., R.D., K.M.C., A.T., K.F., R.U., M.S., D.Q., J.W.S., N.L.C., J.T., J.K., Y.-W.C., A.R., B.A.G. and M.B. performed experiments. C.C.M. performed the blinded pathologic assessment. A.E.H., J.D.O., M.R.P., Y.T., K.M.C., A.T., M.S., J.A.R., E.C.R., D.Q. and H.-W.S. analyzed data. A.E.H., J.D.O., G.V.-N. and M.B. co-wrote the manuscript.

Competing interests

The authors declare no competing interests.

Additional information

Extended data is available for this paper at https://doi.org/10.1038/s41591-020-0971-8.

Supplementary information is available for this paper at https://doi.org/10.1038/s41591-020-0971-8.

Correspondence and requests for materials should be addressed to M.B. or G.V.-N.

Reprints and permissions information is available at www.nature.com/reprints.

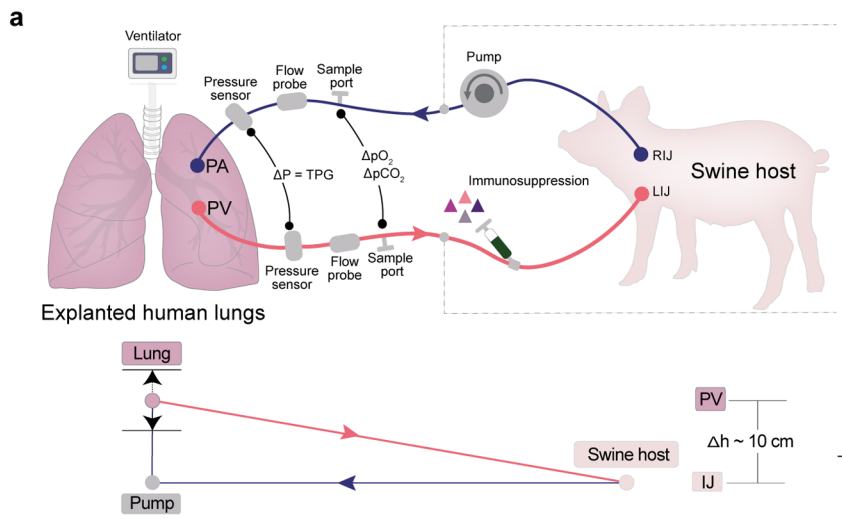

Pulmonary artery (PA)	
Pressure (mmHg)	**15.7** ± 4.7
Flow (mL min^{-1})	**260** ± 95
Swine (bioreactor component)	
Heart rate (beats min^{-1})	**102** ± 2.0
Systolic BP (mmHg)	**88** ± 3.0
pH	**7.43** ± 0.04
Lactate (mmol L^{-1})	**1.6** ± 0.09
Pulmonary vein (PV)	
Pressure (mmHg)	**3.4** ± 2.0
Flow (mL min^{-1})	**260** ± 95
Temperature (ºC)	**35.4** ± 0.2
Transpulmonary pressure gradient	
TPG (mmHg)	**12.3** ± 4.7

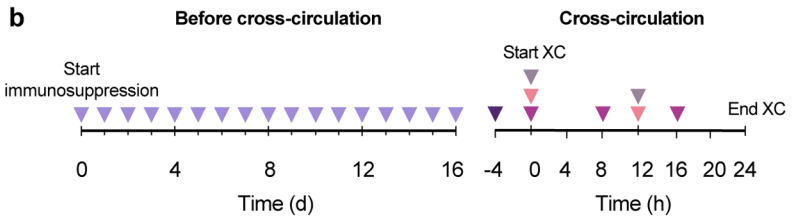

Before cross-circulation	Mycophenolate, PO	500 mg
	Tacrolimus, PO	0.4 mg kg^{-1}
Cross-circulation	Cobra venom factor, IV	1 mg
	Methylprednisolone, IV	125 mg
	Mycophenolate, IV	500 mg
	Tacrolimus, IV	5 mg

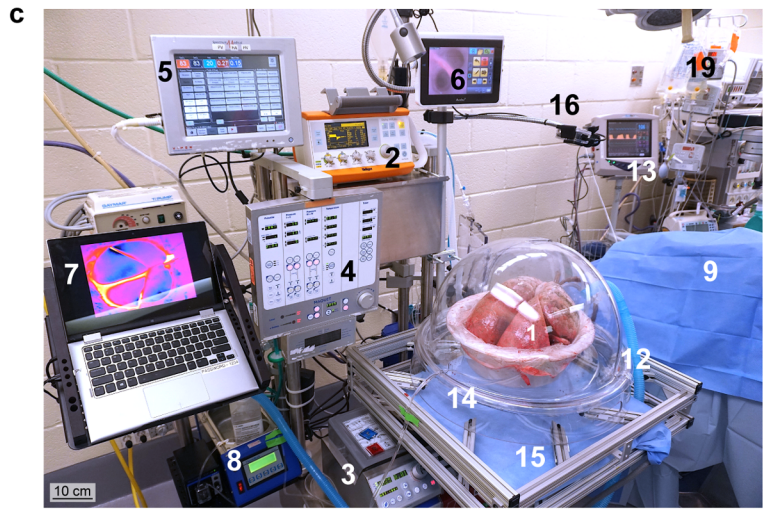

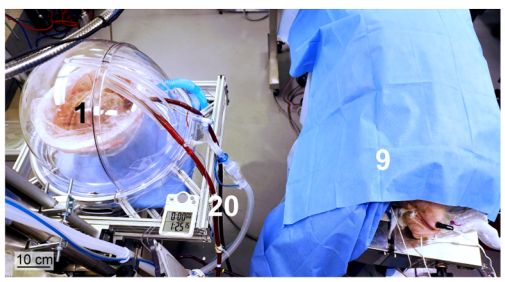

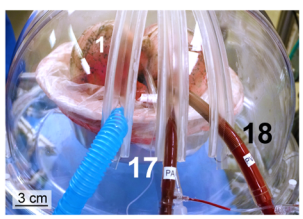

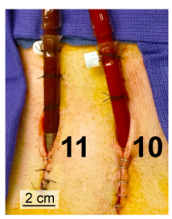

1 Explanted human lungs
2 Ventilator
3 Perfusion controls
4 Perfusion data display
5 Perfusion data aquisition system
6 Video bronchoscopy
7 Thermography
8 Recirculating warm water reservoir
9 Swine host
10 Swine host cannulation site (inflow)
11 Swine host cannulation site (outflow)
12 Humidification system
13 Vitals monitor (swine host)
14 Organ support platform
15 X-ray plate
16 Time-lapse photography
17 Pulmonary artery (inflow)
18 Pulmonary vein (outflow)
19 Intravenous infusions (swine host)
20 Perfusion circuit tubing

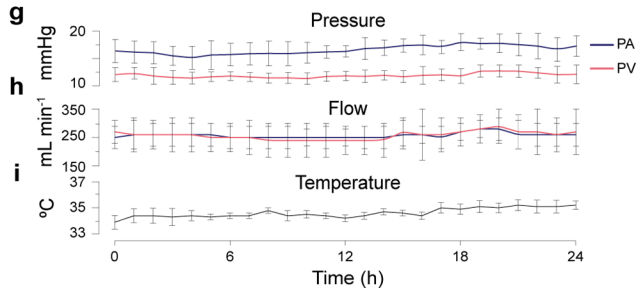

Extended Data Fig. 1 | Experimental setup and xenogeneic cross-circulation circuit parameters. a, Schematic of xenogeneic cross-circulation with mean values of perfusion circuit parameters. To maintain pulmonary vein drainage, lungs were positioned approximately 10 cm higher than swine hosts (Δh). **b**, Immunosuppression regimen, including induction immunosuppression before cross-circulation and maintenance immunosuppression during cross-circulation. **c**, Experimental setup during xenogeneic cross-circulation procedure. **d**, Perfusion circuit connecting the vascular compartments of explanted human lungs and anesthetized swine host. **e**, Pulmonary artery and vein cannulas connecting explanted human lungs to the xenogeneic cross-circulation circuit. **f**, Swine host neck cannulation sites. Extracorporeal circuit parameters: **g**, Pressure. **h**, Flow. **i**, Temperature. All graphs represent data for human lungs ($n = 5$ independent experiments). All values represent mean ± standard deviation.

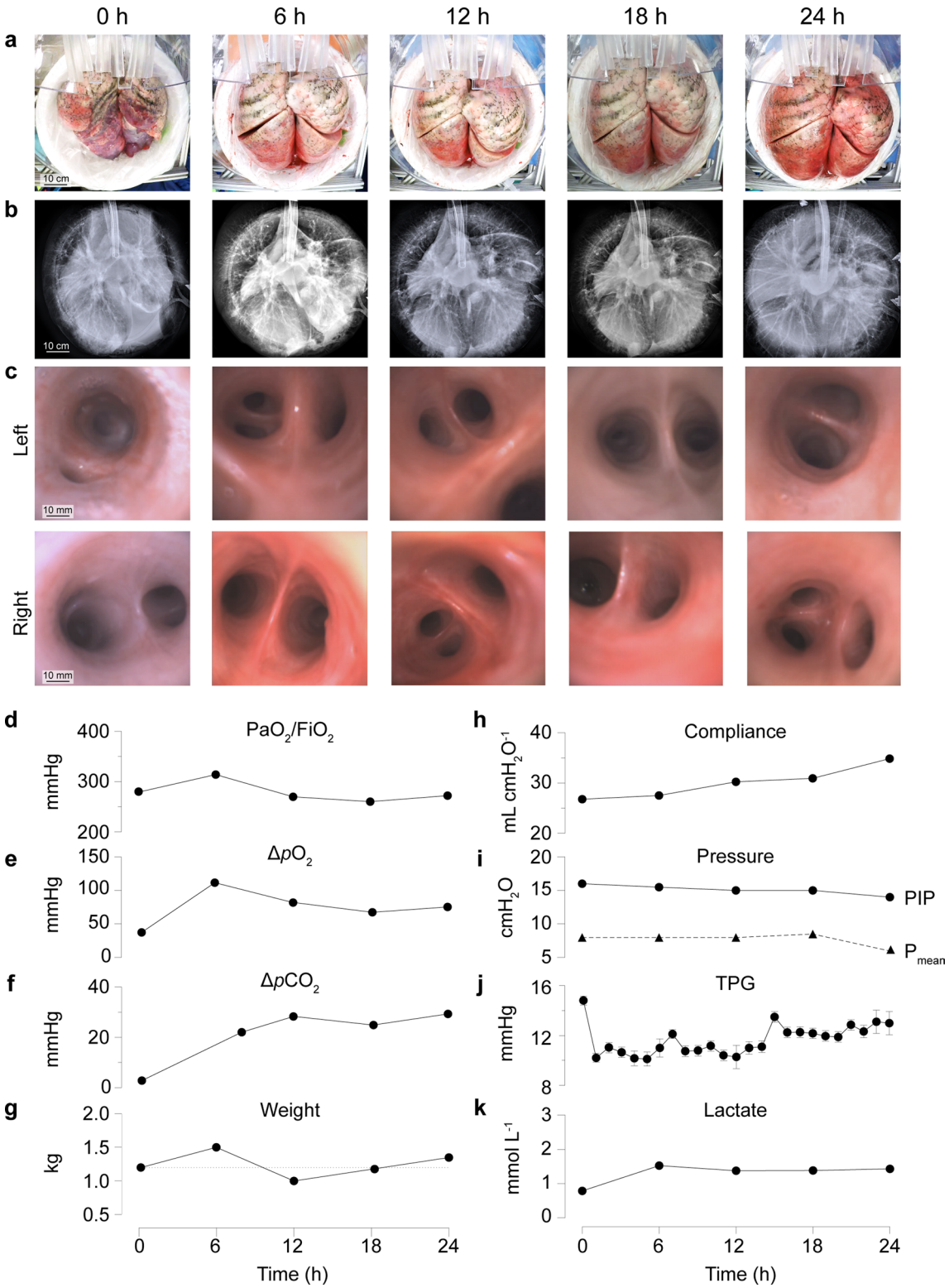

Extended Data Fig. 2 | Multi-scale analyses of human lung 1. a, Gross photography. **b**, Radiography. **c**, Bronchoscopy of left and right lung. **d**, PaO_2/FiO_2. **e**, Change in pO_2 ($\Delta p = |p_{PA} - p_{PV}|$). **f**, Change in pCO_2 ($\Delta p = |p_{PA} - p_{PV}|$). **g**, Lung weight. **h**, Dynamic compliance. **i**, Peak inspiratory pressure (PIP). **j**, Transpulmonary pressure gradient (TPG). **k**, Lactate. All graphs represent images and data for human lung 1 ($n = 1$ independent experiment). **e**-**i**, **k**, Data points represent a single value obtained at each time point. **j**, Data points represent mean ± standard deviation of all values obtained at each time point.

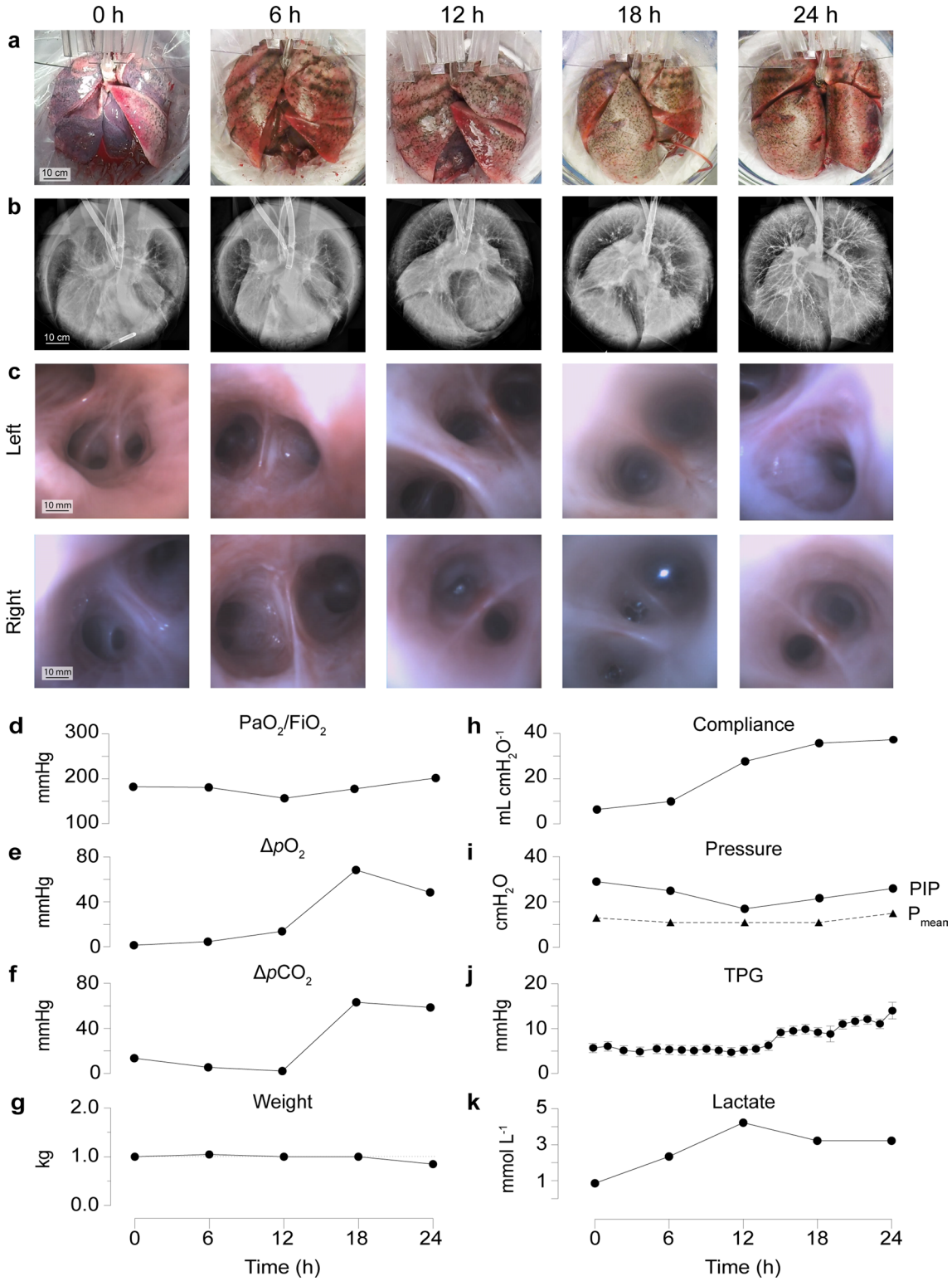

Extended Data Fig. 3 | Multi-scale analyses of human lung 2. a, Gross photography. **b**, Radiography. **c**, Bronchoscopy of left and right lung. **d**, PaO_2/FiO_2. **e**, Change in pO_2 ($\Delta p = |p_{PA} - p_{PV}|$). **f**, Change in pCO_2 ($\Delta p = |p_{PA} - p_{PV}|$). **g**, Lung weight. **h**, Dynamic compliance. **i**, Peak inspiratory pressure (PIP). **j**, Transpulmonary pressure gradient (TPG). **k**, Lactate. All graphs represent images and data for human lung 2 ($n = 1$ independent experiment). **e**-**i**, **k**, All data points represent a single value obtained at each time point. **j**, Data points represent mean ± standard deviation of all values obtained at each time point.

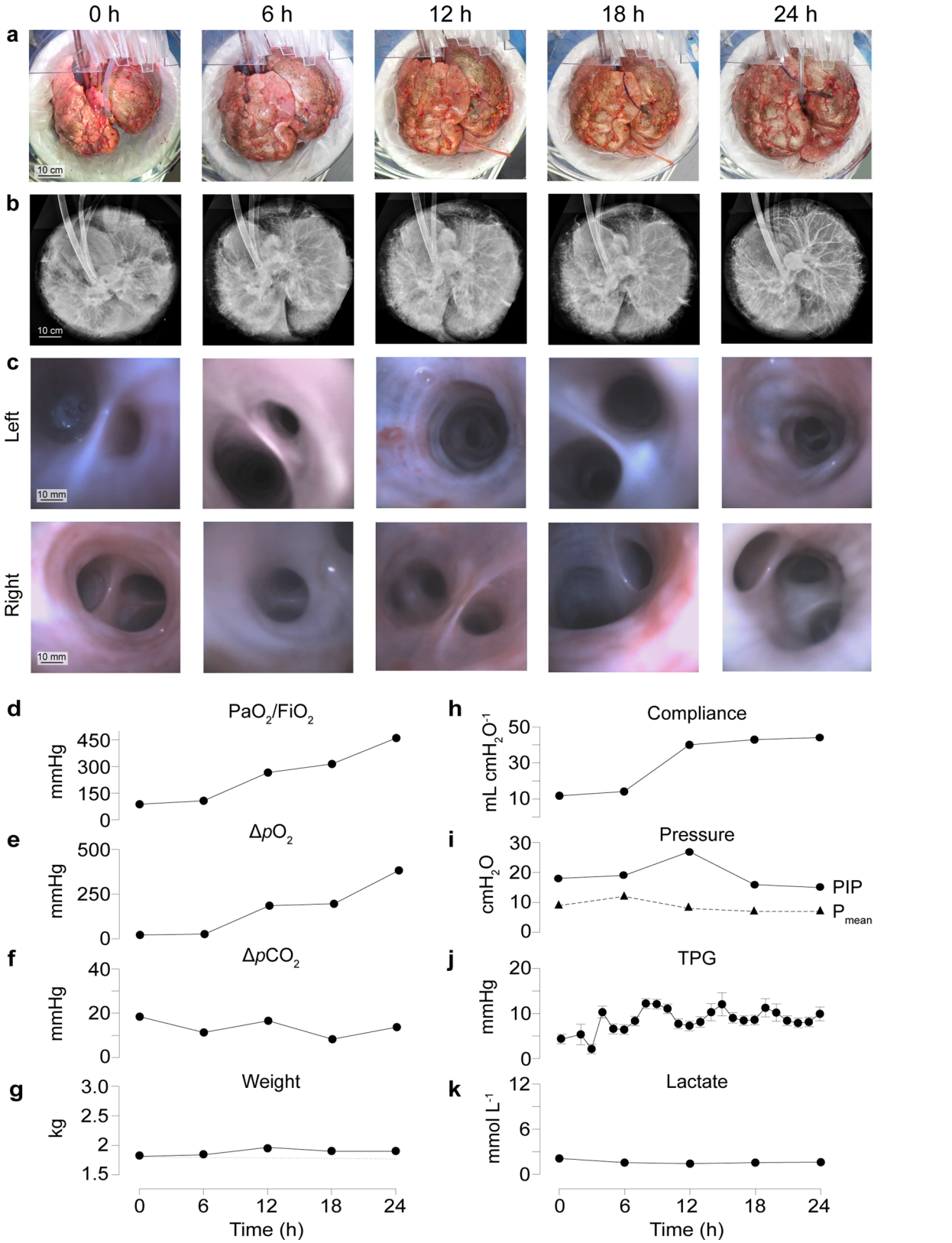

Extended Data Fig. 4 | Multi-scale analyses of human lung 3. a, Gross photography. **b**, Radiography. **c**, Bronchoscopy of left and right lung. **d**, PaO_2/FiO_2. **e**, Change in pO_2 ($\Delta p = |p_{PA} - p_{PV}|$). **f**, Change in pCO_2 ($\Delta p = |p_{PA} - p_{PV}|$). **g**, Lung weight. **h**, Dynamic compliance. **i**, Peak inspiratory pressure (PIP). **j**, Transpulmonary pressure gradient (TPG). **k**, Lactate. All graphs represent images and data for human lung 3 ($n = 1$ independent experiment). **e**-**i**, **k**, All data points represent a single value obtained at each time point. j, Data points represent mean ± standard deviation of all values obtained at each time point.

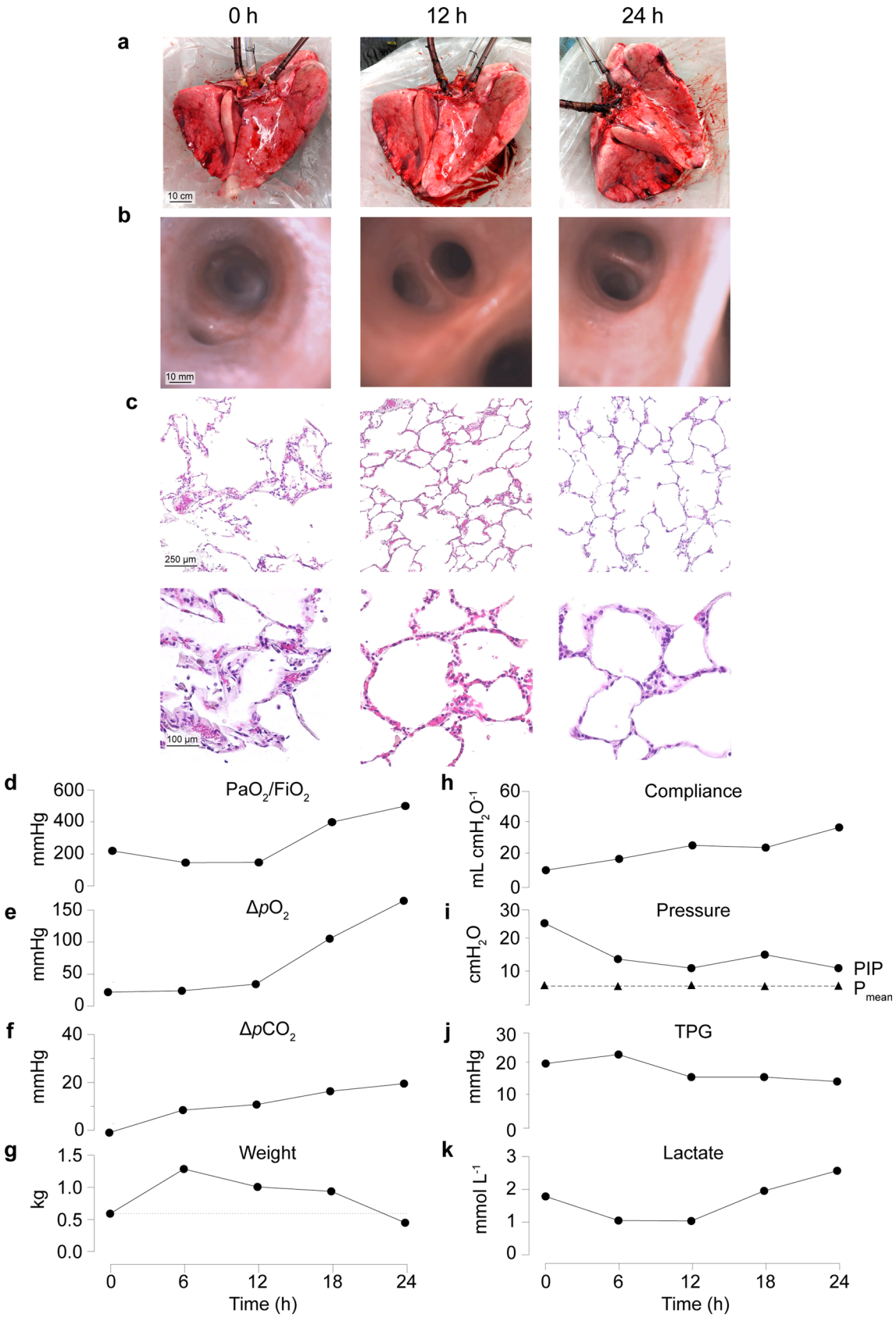

Extended Data Fig. 5 | Multi-scale analyses of human lung 4. a, Gross photography. **b**, Bronchoscopy. **c**, Histologic staining with hematoxylin and eosin. **d**, PaO_2/FiO_2. **e**, Change in pO_2 ($\Delta p = |p_{PA} - p_{PV}|$). **f**, Change in pCO_2 ($\Delta p = |p_{PA} - p_{PV}|$). **g**, Lung weight. **h**, Dynamic compliance. **i**, Peak inspiratory pressure (PIP). **j**, Transpulmonary pressure gradient (TPG). **k**, Lactate. All graphs represent images and data for human lung 4 ($n = 1$ independent experiment). **d**-**k**, All data points represent a single value obtained at each time point.

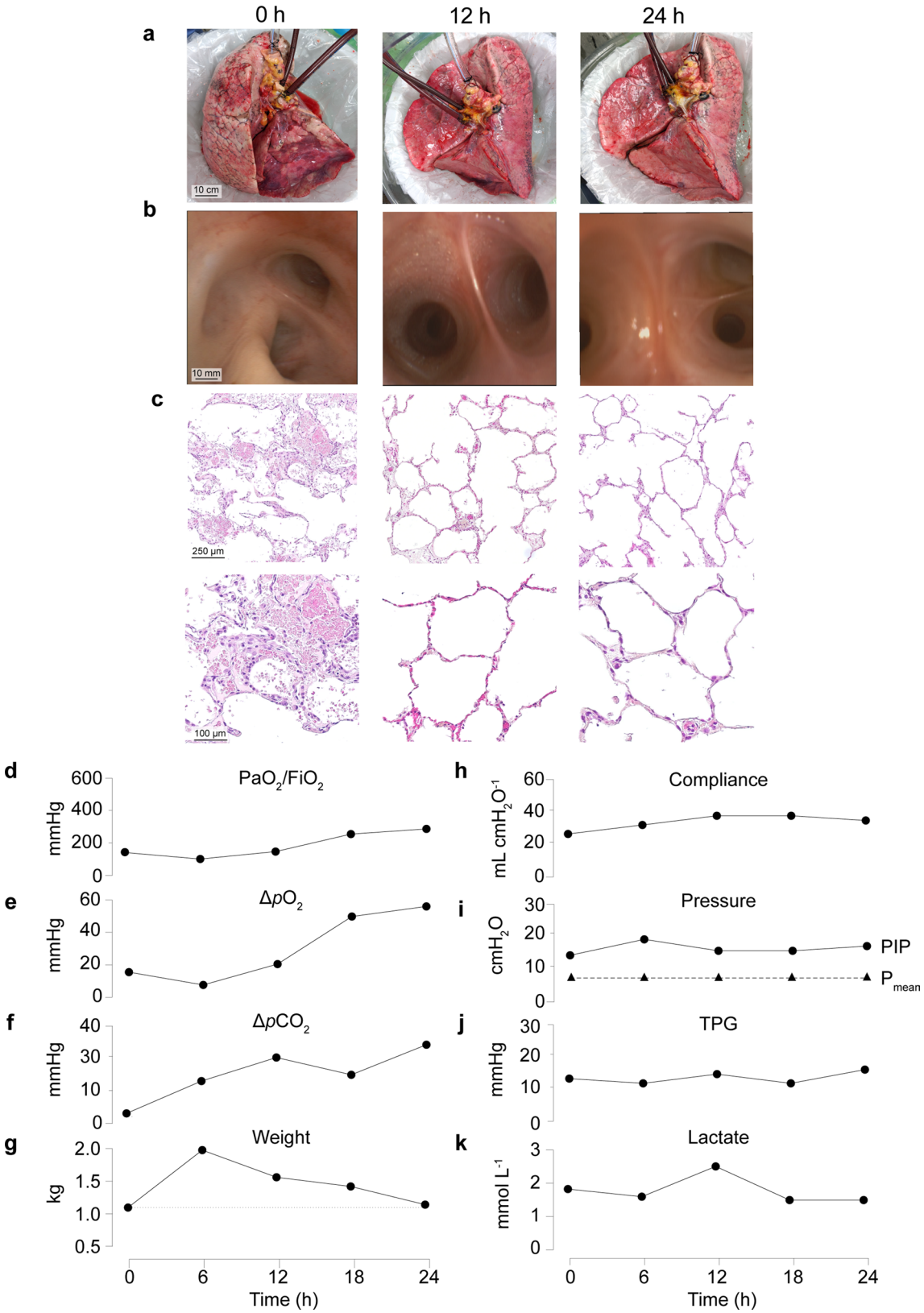

Extended Data Fig. 6 | Multi-scale analyses of human lung 5. a, Gross photography. **b**, Bronchoscopy. **c**, Histologic staining with hematoxylin and eosin. **d**, PaO_2/FiO_2. **e**, Change in pO_2 ($\Delta p = |p_{PA} - p_{PV}|$). **f**, Change in pCO_2 ($\Delta p = |p_{PA} - p_{PV}|$). **g**, Lung weight. **h**, Dynamic compliance. **i**, Peak inspiratory pressure (PIP). **j**, Transpulmonary pressure gradient (TPG). **k**, Lactate. All graphs represent images and data for human lung 5 ($n = 1$ independent experiment). **d**-**k**, All data points represent a single value obtained at each time point.

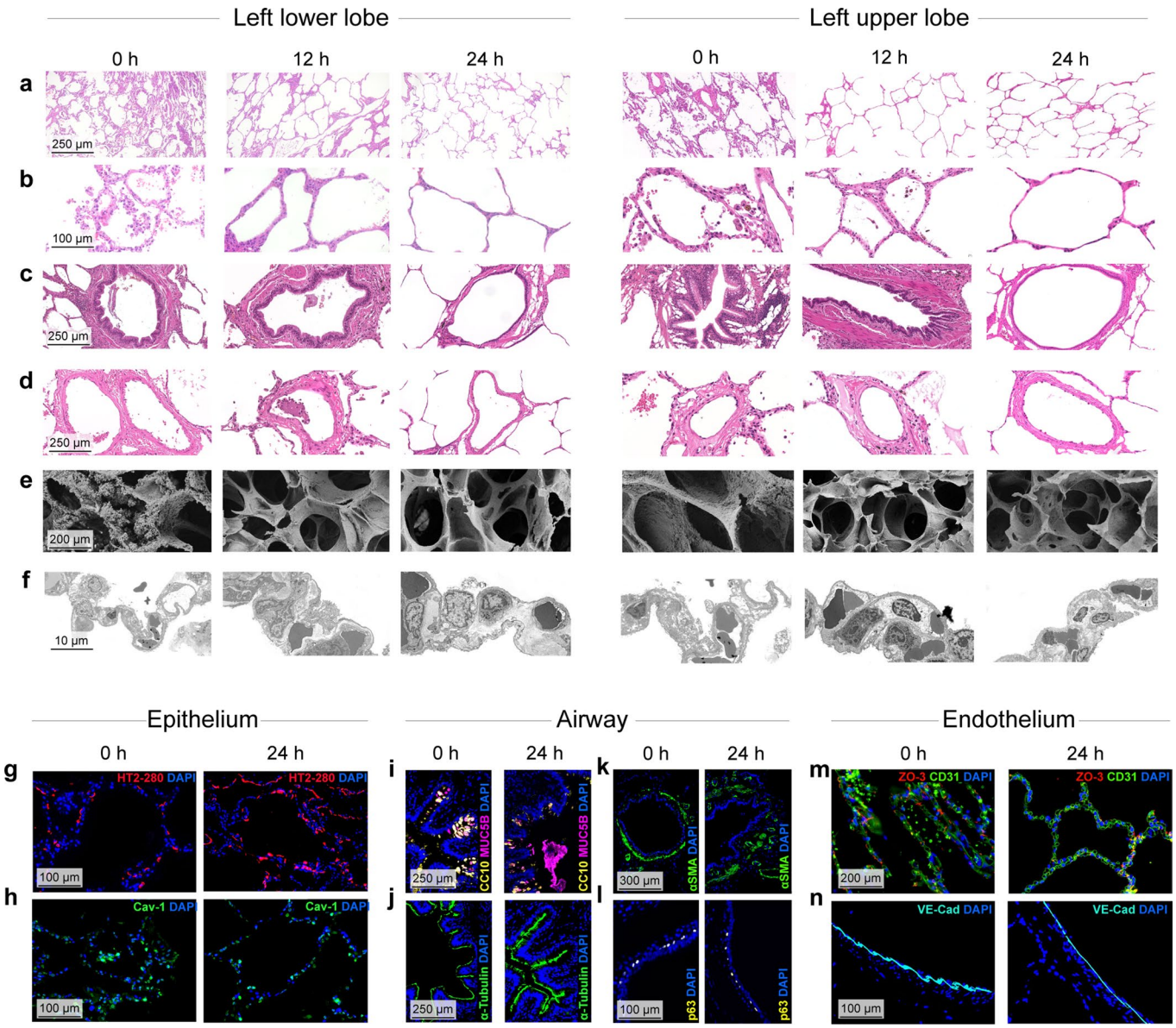

Extended Data Fig. 7 | Histologic evaluation of human lung 1. Micrographs of hematoxylin and eosin staining of upper and lower lobes. **a**, Lung parenchyma at low magnification. **b**, Lung parenchyma at high magnification. **c**, Small airways. **d**, Pulmonary vessels. **e**, Scanning electron micrographs of alveoli. **f**, Transmission electron micrographs of alveolar septa. Immunohistochemical staining of: **g**, HT2-280$^+$ type II pneumocytes. **h**, Caveolin-1$^+$ type I pneumocytes. **i**, CC10$^+$ club cells and Mucin 5B$^+$ goblet cells. **j**, α-tubulin$^+$ ciliated cells. **k**, α-SMA$^+$ submucosal glands. **l**, p63$^+$ basal cells. **m**, CD31$^+$ microvascular endothelial cells and ZO-3$^+$ epithelial tight junctions. **n**, Vascular endothelial (VE)-Cadherin$^+$ endothelial cells.

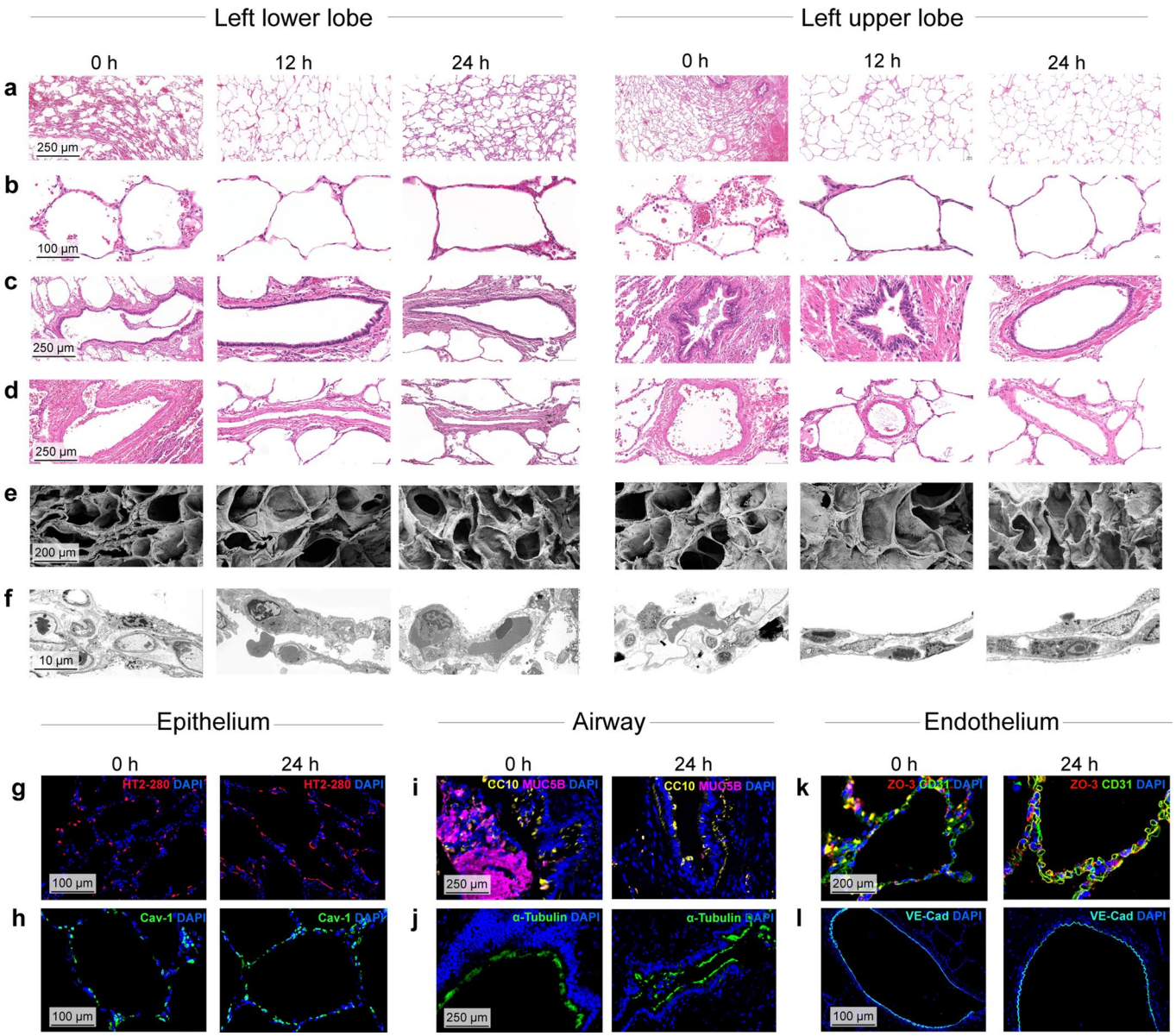

Extended Data Fig. 8 | Histologic evaluation of human lung 2. Micrographs of hematoxylin and eosin staining of upper and lower lobes: **a**, Lung parenchyma at low magnification. **b**, Lung parenchyma at high magnification. **c**, Small airways. **d**, Pulmonary vessels. **e**, Scanning electron micrographs of alveoli. **f**, Transmission electron micrographs of alveolar septa. Immunohistochemical staining of: **g**, HT2-280$^+$ type II pneumocytes. **h**, Caveolin-1$^+$ type I pneumocytes. **i**, CC10$^+$ club cells and Mucin 5B$^+$ goblet cells. **j**, α-tubulin$^+$ ciliated cells. **k**, CD31$^+$ microvascular endothelial cells and ZO-3$^+$ epithelial tight junctions. **l**, Vascular endothelial (VE)-Cadherin$^+$ endothelial cells.

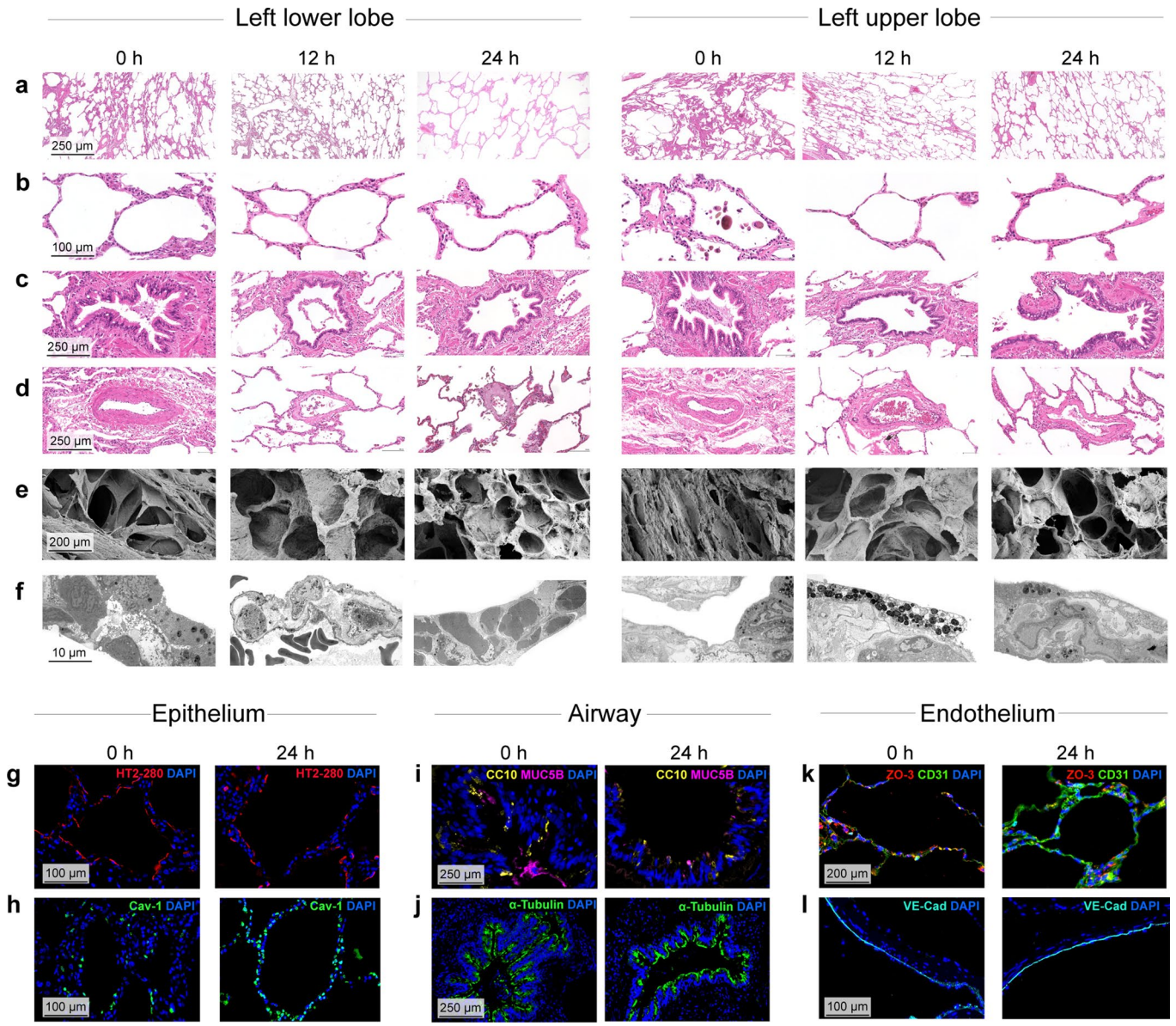

Extended Data Fig. 9 | Histologic evaluation of human lung 3. Micrographs of hematoxylin and eosin staining of upper and lower lobes: **a**, Lung parenchyma at low magnification. **b**, Lung parenchyma at high magnification. **c**, Small airways. **d**, Pulmonary vessels. **e**, Scanning electron micrographs of alveoli. **f**, Transmission electron micrographs of alveolar septa. Immunohistochemical staining of: **g**, HT2-280$^+$ type II pneumocytes. **h**, Caveolin-1$^+$ type I pneumocytes. **i**, CC10$^+$ club cells and Mucin 5B$^+$ goblet cells. **j**, α-tubulin$^+$ ciliated cells. **k**, CD31$^+$ microvascular endothelial cells and ZO-3$^+$ epithelial tight junctions. **l**, Vascular endothelial (VE)-Cadherin$^+$ endothelial cells.

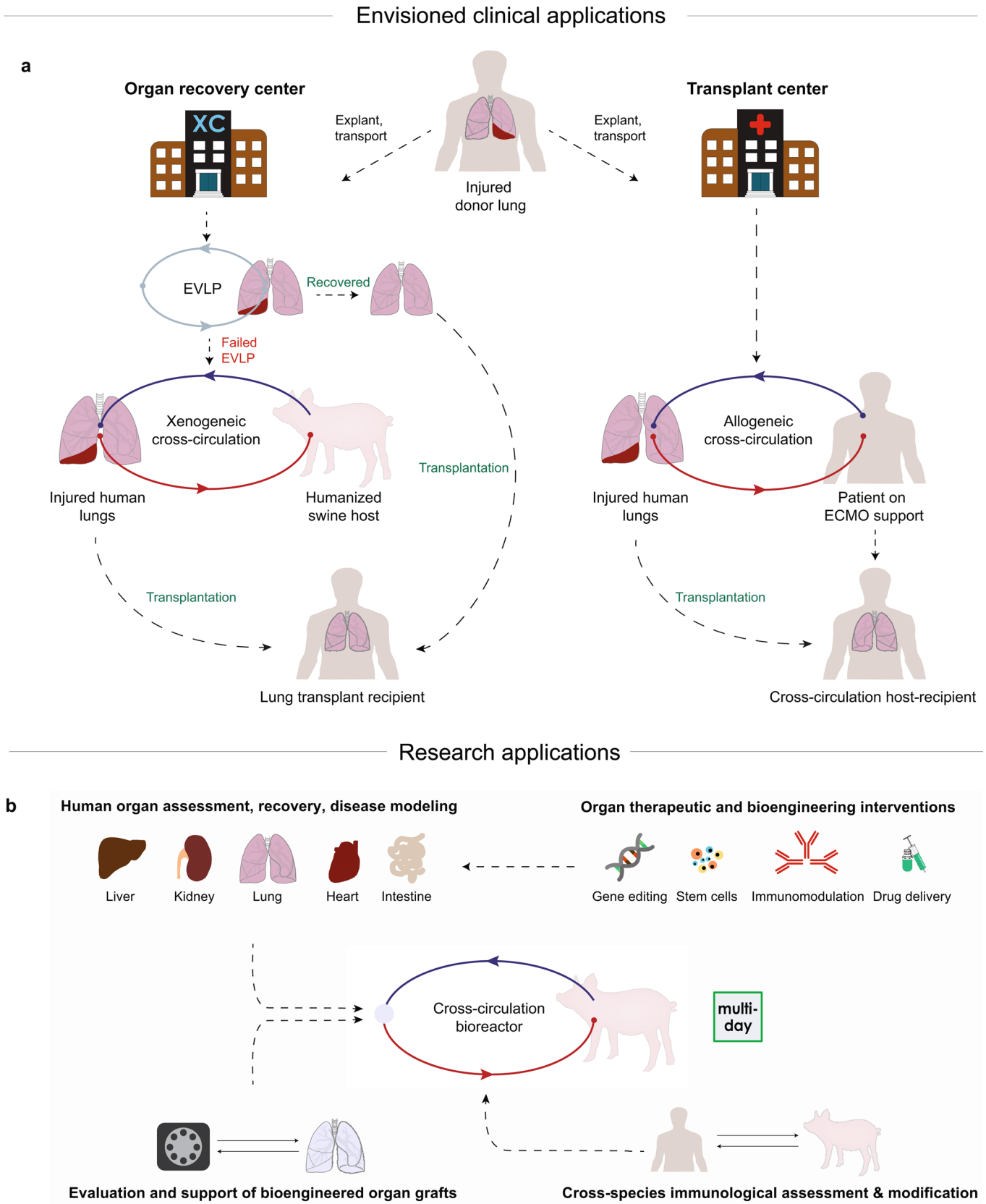

Extended Data Fig. 10 | Envisioned applications of xenogeneic cross-circulation platform. a, Clinical applications of human lungs recovered using xenogeneic cross-circulation. Injured human lungs can be recovered at organ recovery or transplant centers. Lungs recovered by cross-circulation could be transplanted into recipient patients awaiting transplantation. **b**, Research applications. Xenogeneic cross-circulation can be used as a physiologic bioreactor to maintain extracorporeal organs or grafts, enabling research and development of bioengineered constructs, advanced therapeutics, disease models, and investigation of cross-species immunological interactions. EVLP, ex vivo lung perfusion. XC, cross-circulation.

nature research

Corresponding author(s): NMED-A100880A

Last updated by author(s): 05/28/2020

Reporting Summary

Nature Research wishes to improve the reproducibility of the work that we publish. This form provides structure for consistency and transparency in reporting. For further information on Nature Research policies, see Authors & Referees and the Editorial Policy Checklist.

Statistics

For all statistical analyses, confirm that the following items are present in the figure legend, table legend, main text, or Methods section.

n/a	Confirmed	
☐	☒	The exact sample size (*n*) for each experimental group/condition, given as a discrete number and unit of measurement
☐	☒	A statement on whether measurements were taken from distinct samples or whether the same sample was measured repeatedly
☐	☒	The statistical test(s) used AND whether they are one- or two-sided *Only common tests should be described solely by name; describe more complex techniques in the Methods section.*
☐	☒	A description of all covariates tested
☐	☒	A description of any assumptions or corrections, such as tests of normality and adjustment for multiple comparisons
☐	☒	A full description of the statistical parameters including central tendency (e.g. means) or other basic estimates (e.g. regression coefficient) AND variation (e.g. standard deviation) or associated estimates of uncertainty (e.g. confidence intervals)
☐	☒	For null hypothesis testing, the test statistic (e.g. *F*, *t*, *r*) with confidence intervals, effect sizes, degrees of freedom and *P* value noted *Give P values as exact values whenever suitable.*
☒	☐	For Bayesian analysis, information on the choice of priors and Markov chain Monte Carlo settings
☒	☐	For hierarchical and complex designs, identification of the appropriate level for tests and full reporting of outcomes
☒	☐	Estimates of effect sizes (e.g. Cohen's *d*, Pearson's *r*), indicating how they were calculated

Our web collection on statistics for biologists contains articles on many of the points above.

Software and code

Policy information about availability of computer code

Data collection	All software used to collect data in this study is commercial or open source software. Each software version is specified in Methods and here: Image Capture Engine v. 602.569 (AMT); VIPER clinical interfacing software G2 v1.26.4 (Spectrum Medical)
Data analysis	All software used to analyze data in this study is commercial or open source software, as specified in Methods and here: ImageJ v. 1.51m9 (NIH); Prism v. 8.2.1 (GraphPad); STAR aligner v. 2.5.2b; Pheatmap v. 1.08; R v. 3.6.0; GeneSCF v. 1.1-p2; Trimmomatic v.0.36 (Usadel Lab)

For manuscripts utilizing custom algorithms or software that are central to the research but not yet described in published literature, software must be made available to editors/reviewers. We strongly encourage code deposition in a community repository (e.g. GitHub). See the Nature Research guidelines for submitting code & software for further information.

Data

Policy information about availability of data

All manuscripts must include a data availability statement. This statement should provide the following information, where applicable:

- Accession codes, unique identifiers, or web links for publicly available datasets
- A list of figures that have associated raw data
- A description of any restrictions on data availability

The authors declare that all data supporting the findings of this study are available within the text, figures, and Supplementary Information.

Field-specific reporting

Please select the one below that is the best fit for your research. If you are not sure, read the appropriate sections before making your selection.

☒ Life sciences ☐ Behavioural & social sciences ☐ Ecological, evolutionary & environmental sciences

For a reference copy of the document with all sections, see nature.com/documents/nr-reporting-summary-flat.pdf

Life sciences study design

All studies must disclose on these points even when the disclosure is negative.

Sample size	The study was designed as a proof-of-feasibility study (n = 6) to assess the ability of the xenogeneic cross-circulation system to maintain and recover the quality and function of explanted human lungs for 24 hours. The study included two experimental groups: (i) with immunosuppression (n = 5), and (ii) without immunosuppression (n = 1 as an immunological control), and was conducted with the minimum number of animals to demonstrate feasibility and reproducibility between lungs and across experimental time points. Data from this study can be used to conduct power analyses for subsequent investigations. All samples were collected and analyzed in duplicate or more.
Data exclusions	No data were excluded from analysis.
Replication	All samples and data from n = 6 experiments were processed and analyzed in parallel. As established experimental models and methods were used, all attempts at replication were successful.
Randomization	Randomization of sampling. To avoid sampling bias, the location of lung wedge tissue sample collections was randomized using a random number generator (www.random.org). Prior to the start of each experiment, a lung map with pre-determined regions (8 regions per left or right lung) was generated, and each region was assigned an arbitrary number, as previously described. Throughout all procedures, samples were collected at each time point according to the lung map regions that corresponded to the randomly generated numbers. Lung wedge tissue samples were collected for histologic, microscopic, and pathologic analyses.
Blinding	All analytical assessments were blinded to the maximum practical extent. All pathologic analyses were performed by an independent expert, in a blinded fashion, to eliminate bias.

Reporting for specific materials, systems and methods

We require information from authors about some types of materials, experimental systems and methods used in many studies. Here, indicate whether each material, system or method listed is relevant to your study. If you are not sure if a list item applies to your research, read the appropriate section before selecting a response.

Materials & experimental systems

n/a	Involved in the study
☐	☒ Antibodies
☒	☐ Eukaryotic cell lines
☒	☐ Palaeontology
☐	☒ Animals and other organisms
☐	☒ Human research participants
☒	☐ Clinical data

Methods

n/a	Involved in the study
☒	☐ ChIP-seq
☒	☐ Flow cytometry
☒	☐ MRI-based neuroimaging

Antibodies

Antibodies used

Antibody: Anti-alpha smooth muscle actin Vendor: ThermoFisher Catalog #: MA1-06110 Clone: 1A4 Lot #: UB2721611 Dilution: 1:100
Antibody: Anti-alpha tubulin Vendor: Cell Signaling Catalog # 2144 Clone: N/A Lot #:6 Dilution: 1:50
Antibody: Anti-aquaporin 5 Vendor: Santa Cruz Catalog # sc-9890 Clone: N/A Lot #: G1316 Dilution: 1:100
Antibody: Anti-C3b Vendor: BioRad Catalog # 0200-9614 Clone: H11 Lot #: 171122 Dilution: 1:150
Antibody: Anti-C5b-9 Vendor: Dako Catalog # M0777 Clone: aE11 Lot #: 20061175 Dilution: 1:200
Antibody: Anti-caspase 3 Vendor: Abcam Catalog # ab13847 Clone: N/A Lot # GR3226155 Dilution: 1:100
Antibody: Anti-caveolin 1 Vendor: ThermoFisher Catalog # MA3-600 Clone: 7C8 Lot # TH271118 Dilution: 1:20
Antibody: Anti-CC10 Vendor: Santa Cruz Catalog # sc-9770 Clone: C-20 Lot # L2016 Dilution: 1:100
Antibody: Anti-CD31 Vendor: Cell Signaling Catalog # 3528 Clone: Lot # 89C2 7 Dilution: 1:500
Antibody: Anti-CD45 Vendor: Abcam Catalog # ab10559 Clone: N/A Lot # GR3245601-1 Dilution: 1:100
Antibody: Anti-CD163 Vendor: Abcam Catalog # ab87099 Clone: N/A Lot # GR3262800 Dilution: 1:100
Antibody: Anti-EpCAM Vendor: Cell Signaling Catalog # 14452S Clone: D9S3P Lot #:1 Dilution: 1:200
Antibody: Anti-factor XIII Vendor: ThermoFisher Catalog # MA5-11751 Clone: UB2711684 Lot # AC-1A1 Dilution: 1:100
Antibody: Anti-galactose-alpha-1,3-galactose (αGal) Vendor: LSBio Catalog #LS-C63415 Clone: M86 Lot # 164158 Dilution: 1:100
Antibody: Anti-HT2-280 Vendor: Terrace Biotech Catalog # TB-27AHT2-280 Clone: N/A Lot # N/A Dilution: 1:150

Antibody: Anti-human nuclear antigen Vendor: Abcam Catalog # ab190710 Clone: NM95 Lot # GR3269017-3 Dilution: 1:100
Antibody: Anti-ITGA2B (CD41) Vendor: LSBio Catalog # LS-B9763-100 Clone: ITGA2B Lot # 40124 Dilution: 1:100
Antibody: Anti-mucin 5B Vendor: Santa Cruz Catalog # sc-20119 Clone: H-300 Lot # J1416 Dilution: 1:100
Antibody: Anti-neutrophil elastase Vendor: Abcam Catalog # ab68672 Clone: N/A Lot # GR286865 Dilution: 1:100
Antibody: Anti-NG2 Vendor: Abcam Catalog # Ab129051 EPR22410-145 Lot # GR3283650-2 Dilution: 1:200
Antibody: Anti-p63 Vendor: Cell Signaling Catalog # 39692 Clone: D9L7L Lot # 1 Dilution: 1:300
Antibody: Anti-PGP9.5 Vendor: Abcam Catalog # ab20559 Clone: 31A3 Lot # GR297419-2 Dilution: 1:200
Antibody: Anti-Sox9 Vendor: Cell Signaling Catalog # 82630S Clone: D8G8H Lot # 1 Dilution: 1:200
Antibody: Anti-SPC Vendor: ABCAM Catalog # 40879 Clone: N/A Lot # GR249444-1 Dilution: 1:200
Antibody: Anti-VE-cadherin Vendor: Abcam Catalog # Ab33168 Clone: N/A Lot # Gr311141-1 Dilution: 1:150
Antibody: Anti-ZO-1 Vendor: ThermoFisher Catalog # ZO1-1A12 Clone: Z01-1A12 Lot # TL275320 Dilution: 1:100
Antibody: Anti-ZO-3 Vendor: ThermoFisher Catalog # 36-4000 Clone: N/A Lot # TD262559 Dilution: 1:200
Antibody: Anti-Goat IgG (528) Vendor: Abcam Catalog # ab6881 Clone: N/A Lot #GR69643 Dilution: 1:200
Antibody: Anti-Mouse IgG (647) Vendor: Abcam Catalog # ab150115 Clone: N/A Lot #GR277379 Dilution: 1:200
Antibody: Anti-Rabbit IgG (594) Vendor: Abcam Catalog # Ab150081 Clone: N/A Lot #GR178296-3 Dilution: 1:200

Validation

All antibodies used in this study were validated. Detailed information can be found on the manufacturers' websites below:

Anti-alpha smooth muscle actin: https://www.thermofisher.com/antibody/product/Alpha-Smooth-Muscle-Actin-Antibody-clone-1A4-Monoclonal/MA1-06110
Anti-alpha tubulin: https://www.cellsignal.com/products/primary-antibodies/a-tubulin-antibody/2144
Anti-aquaporin 5: https://www.scbt.com/p/aqp5-antibody-g-19
Anti-C3b: https://www.bio-rad-antibodies.com/monoclonal/human-c3b-antibody-h11-0200-0614.html?f=purified
Anti-C5b-9: https://www.labome.com/product/Dako/M0777.html
Anti-caspase 3:https://www.abcam.com/caspase-3-antibody-ab13847.html
Anti-caveolin 1: https://www.thermofisher.com/antibody/product/Caveolin-1-Antibody-clone-7C8-Monoclonal/MA3-600
Anti-CC10: https://www.scbt.com/p/cc10-antibody-c-20
Anti-CD31: https://www.cellsignal.com/products/primary-antibodies/cd31-pecam-1-89c2-mouse-mab/3528
Anti-CD45: https://www.abcam.com/cd45-antibody-hematopoietic-stem-cell-marker-ab10559.html
Anti-CD163: https://www.abcam.com/cd163-antibody-ab87099.html
Anti-EpCAM: https://www.cellsignal.com/products/primary-antibodies/epcam-d9s3p-rabbit-mab-ihc-preferred/14452
Anti-factor XIII: https://www.thermofisher.com/antibody/product/Factor-XIII-A-Antibody-clone-AC-1A1-Monoclonal/MA5-11751
Anti-galactose-alpha-1,3-galactose (αGal): https://www.lsbio.com/antibodies/alpha-gal-epitope-antibody-clone-m86-elisa-flow-ihc-wb-western-ls-c63415/64041
Anti-HT2-280: https://www.terracebiotech.com/product-page/anti-ht2-280-1ml
Anti-human nuclear antigen: https://www.abcam.com/human-nucleoli-antibody-nm95-nucleolar-marker-ab190710.html
Anti-ITGA2B (CD41): https://www.lsbio.com/antibodies/ihc-plus-itga2b-antibody-cd41-antibody-aa122-171-ihc-wb-western-ls-b9763/212790
Anti-mucin 5B: https://www.scbt.com/p/mucin-5b-antibody-h-300
Anti-neutrophil elastase: https://www.abcam.com/neutrophil-elastase-antibody-ab68672.html
Anti-NG2: https://www.abcam.com/ng2-antibody-ab129051.html
Anti-p63: https://www.cellsignal.com/products/primary-antibodies/p63-d9l7l-xp-rabbit-mab/39692
Anti-PGP9.5: https://www.abcam.com/pgp95-antibody-31a3-ab20559.html
Anti-Sox9: https://www.cellsignal.com/products/primary-antibodies/sox9-d8g8h-rabbit-mab/82630
Anti-SPC: https://www.abcam.com/prosurfactant-protein-c-antibody-ab40879.html
Anti-VE-cadherin: https://www.abcam.com/ve-cadherin-antibody-intercellular-junction-marker-ab33168.html
Anti-ZO-1: https://www.thermofisher.com/antibody/product/ZO-1-Antibody-clone-ZO1-1A12-Monoclonal/33-9100
Anti-ZO-3: https://www.thermofisher.com/antibody/product/ZO-3-Antibody-Polyclonal/36-4000
Anti-Goat IgG: https://www.abcam.com/donkey-goat-igg-hl-fitc-ab6881.html
Anti-Mouse IgG: https://www.abcam.com/goat-mouse-igg-hl-alexa-fluor-647-ab150115.html
Anti-Rabbit IgG: https://www.abcam.com/goat-rabbit-igg-hl-alexa-fluor-488-preadsorbed-ab150081.html

Animals and other organisms

Policy information about studies involving animals; ARRIVE guidelines recommended for reporting animal research

Laboratory animals

Species: Sus scrofa domesticus
Sex: Male
Strain: Yorkshire
Age: 5 – 8 months
Weight: 61.4 – 64.0 kg

Wild animals

This study did not involve wild animals.

Field-collected samples

This study did not involve field-collected samples.

Ethics oversight

The xenogeneic cross-circulation procedures were conducted at Columbia University and Vanderbilt University, under protocols approved by the Institutional Animal Care and Use Committee (IACUC) at both Columbia University and Vanderbilt University. All animal care and procedures were conducted in accordance with the US National Research Council of the National Academies Guide for the Care and Use of Laboratory Animals, Eighth Edition.

Note that full information on the approval of the study protocol must also be provided in the manuscript.

Human research participants

Policy information about studies involving human research participants

Population characteristics	Detailed description of the human donors lungs used in this study is provided in Table 1.
Recruitment	Human lungs were recruited through the local Organ Procurement Organization (OPO) in New York, New York or Nashville, Tennessee. A patient (or healthcare proxy) who provided informed consent to donate their organs for research use at the time of death was identified by the OPO, who subsequently contacted our research group at Columbia University and Vanderbilt University to offer donated human lungs not usable for clinical transplantation for research use in xenogeneic cross-circulation studies. The following exclusion criteria were applied: severe purulent secretions on bronchoscopy; history of infection with human immunodeficiency virus (HIV), hepatitis B, hepatitis C, or methicillin-resistant staphylococcus aureus (MRSA).
Ethics oversight	All xenogeneic cross-circulation studies were conducted at Columbia University and Vanderbilt University under protocols classified by the Institutional Review Board (IRB) at each institution as "Not Human Subjects Research". As this study involved no identifying information, and no interaction or intervention between the investigators and any human subjects, the research activity did not meet the definition of human subjects research under the purview of the IRB according to Title 45 CFR part 46, NYS Article 24A, or FDA regulations.

Note that full information on the approval of the study protocol must also be provided in the manuscript.